Tectonophysics 677–678 (2016) 227–240

Contents lists available at ScienceDirect

Tectonophysics

journal homepage: www.elsevier.com/locate/tecto

Continental deformation accommodated by non-rigid passive bookshelf faulting: An example from the Cenozoic tectonic development of northern Tibet

Andrew V. Zuza [a,*], An Yin [a,b]

[a] Department of Earth, Planetary, and Space Sciences, University of California, Los Angeles, CA 90095-1567, USA
[b] Structural Geology Group, China University of Geosciences (Beijing), Beijing 10085, China

ARTICLE INFO

Article history:
Received 9 June 2015
Received in revised form 21 March 2016
Accepted 3 April 2016
Available online 14 April 2016

Keywords:
Bookshelf faulting
Tibetan Plateau
Strike-slip faulting
Kunlun fault
Qinling fault
Haiyuan fault

ABSTRACT

Collision-induced continental deformation commonly involves complex interactions between strike-slip faulting and off-fault deformation, yet this relationship has rarely been quantified. In northern Tibet, Cenozoic deformation is expressed by the development of the >1000-km-long east-striking left-slip Kunlun, Qinling, and Haiyuan faults. Each have a maximum slip in the central fault segment exceeding 10s to ~100 km but a much smaller slip magnitude (~<10% of the maximum slip) at their terminations. The along-strike variation of fault offsets and pervasive off-fault deformation create a strain pattern that departs from the expectations of the classic plate-like rigid-body motion and flow-like distributed deformation end-member models for continental tectonics. Here we propose a non-rigid bookshelf-fault model for the Cenozoic tectonic development of northern Tibet. Our model, quantitatively relating discrete left-slip faulting to distributed off-fault deformation during regional clockwise rotation, explains several puzzling features, including the: (1) clockwise rotation of east-striking left-slip faults against the northeast-striking left-slip Altyn Tagh fault along the northwestern margin of the Tibetan Plateau, (2) alternating fault-parallel extension and shortening in the off-fault regions, and (3) eastward-tapering map-view geometries of the Qimen Tagh, Qaidam, and Qilian Shan thrust belts that link with the three major left-slip faults in northern Tibet. We refer to this specific non-rigid bookshelf-fault system as a passive bookshelf-fault system because the rotating bookshelf panels are detached from the rigid bounding domains. As a consequence, the wallrock of the strike-slip faults deforms to accommodate both the clockwise rotation of the left-slip faults and off-fault strain that arises at the fault ends. An important implication of our model is that the style and magnitude of Cenozoic deformation in northern Tibet vary considerably in the east–west direction. Thus, any single north–south cross section and its kinematic reconstruction through the region do not properly quantify the complex deformational processes of plateau formation.

1. Introduction

The fundamental mode of continental tectonics has been characterized by two end-member processes: plate-like rigid-body motion (e.g., Tapponnier et al., 1982; Weldon and Humphreys, 1986; Avouac and Tapponnier, 1993; Meade, 2007) and distributed deformation via viscous flow (e.g., England and Houseman, 1986; Yin and Taylor, 2011). In the rigid-plate model, continental deformation is quantified by rigid block rotation on a sphere about their respective Euler poles; the horizontal dimension of the blocks is much greater than the width of faults/shear zones that bound the blocks (e.g., Avouac and Tapponnier, 1993). In contrast, the viscous-flow model quantifies continental deformation by solving a boundary-value problem that requires the knowledge of lithospheric rheology (e.g., England and Houseman, 1986). This model envisions distributed continental deformation, with major faults approximated as zones of high strain within a continuum. These two end-member models have been extensively tested in Tibet against structures created during the Cenozoic India–Eurasia collision (e.g., Yin and Harrison, 2000; Zhu et al., 2005; Yin, 2010a; van Hinsbergen et al., 2011; Yin and Taylor, 2011). Debates have been centered on whether the >1000-km-long east-striking left-slip Haiyuan, Qinling, and Kunlun faults in northern Tibet (Fig. 1) have acted as rigid-block boundaries (Tapponnier et al., 1982; Avouac and Tapponnier, 1993; Tapponnier et al., 2001) or transfer-fault structures linking dip-slip fault systems (e.g., Burchfiel et al., 1991; Yin, 2000; Duvall and Clark, 2010).

One form of rigid-block models for deformation in northern Tibet is bookshelf faulting, which requires that the observed left-slip faulting is driven by regional right-lateral shear (Cobbold and Davy, 1988; England and Molnar, 1990). Applying the classic rigid

* Corresponding author.
E-mail addresses: azuza@ucla.edu, avz5818@gmail.com (A.V. Zuza).

http://dx.doi.org/10.1016/j.tecto.2016.04.007
0040-1951/

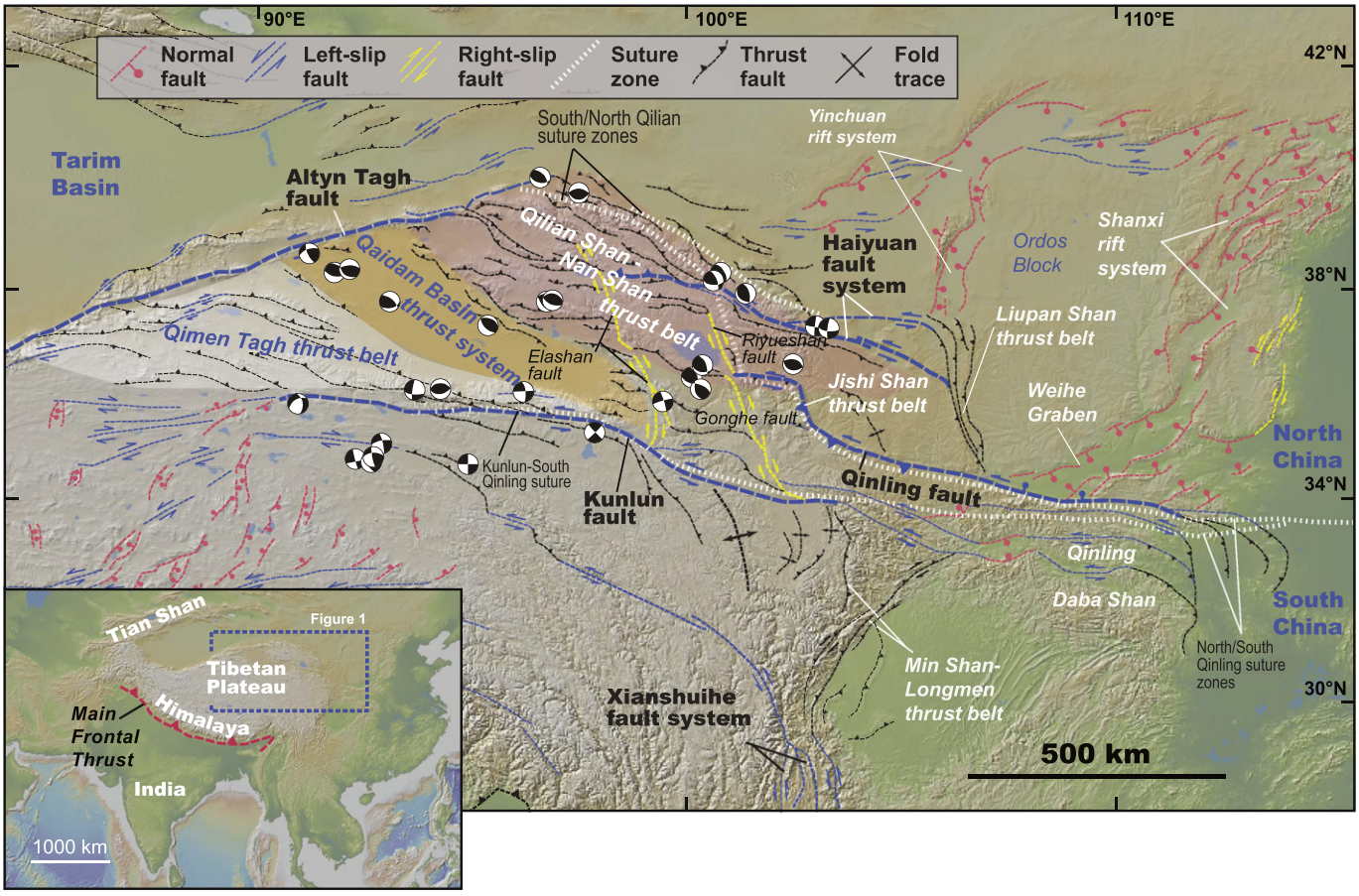

Fig. 1. Color-shaded relief map showing Cenozoic faults related to the India–Eurasia collision zone after Yin et al. (2008a); Taylor and Yin (2009), and Zuza et al. (2016). Also shown are Harvard centroid moment tensor (CMT) earthquake focal mechanisms from 1 January 1977 to 1 January 2009 of events >M5.5. Inset shows location of northern Tibet in the context of the Himalayan–Tibetan orogen. The digital topographic basemap is from the GeoMapApp software (Ryan et al., 2009) available at http://www.geomapapp.org/.

bookshelf-fault model (Freund, 1970) to explain the tectonic development of northern Tibet raises several important questions that have not yet been addressed: (1) Why do the parallel east-striking left-slip faults terminate at the northeast-striking left-slip Altyn Tagh fault rather than a right-slip northeast-striking shear zone as required by the bookshelf-fault model (Fig. 1)? (2) How are the required lithospheric-scale "gaps" and "overlaps" at the ends of the rotating blocks accommodated by off-strike-slip-fault deformation (e.g., Luyendyk et al., 1980; Onderdonk, 2005; Platt and Becker, 2013) (Fig. 2)? (3) What is the kinematic relationship between the east-striking left-slip faults and the triangular eastward-tapering thrust belts at the western ends of the strike-slip faults (i.e., the Qimen Tagh, Qaidam, and Qilian Shan-Nan Shan thrust belts) (Fig. 1)?

In this study we propose a non-rigid bookshelf-fault model (e.g., Yin and Pappalardo, 2015) to resolve the above issues. Specifically, we show that an eastward decrease in Cenozoic strain results in clockwise rotation and left-slip bookshelf faulting across northern Tibet. The detached rotation of these bookshelf faults against rigid bounding domains, a process which we refer to as passive bookshelf faulting, may explain why a left-slip bookshelf fault system is bounded by the left-slip Altyn Tagh fault (Fig. 1). Non-rigid wallrock deformation within the strike-slip-fault-bounded regions accommodates both the clockwise rotation of the strike-slip faults and the space issues that arise at the ends of the bookshelf panels. The model implies that thrust belt development and strike-slip faulting in the region are coeval and kinematically linked, which contrasts an earlier suggestion that they represent two distinct stages of plateau development (e.g., Yuan et al., 2013).

2. Cenozoic left-slip faults in northern Tibet

The ~N110°E-striking left-slip Kunlun, Qinling, and Haiyuan faults, extending for ~1500, ~1000, and ~1000 km respectively, are by far the longest and most continuous structures in northern Tibet (Fig. 1) (Tapponnier et al., 2001; Taylor and Yin, 2009). The faults are lithospheric structures (Wang et al., 2011; Gao et al., 2013) that closely follow the surface traces of the Paleozoic and Mesozoic Qilian, Qinling, and Kunlun suture zones (Yin and Harrison, 2000; Wu et al., in press) (Fig. 1).

The kinematics of these major east-striking faults has been related to lateral extrusion (Tapponnier et al., 1982, 2001; Cheng et al., 2015), strain transfer between thrust belts (Burchfiel et al., 1991; Zhang et al., 1991; Duvall and Clark, 2010), and bookshelf faulting associated with clockwise fault rotation induced by broad and distributed north-trending right-lateral shear (England and Molnar, 1990; Zuza and Yin, 2013) (Fig. 3**a**). The extrusion fault model requires high slip rates (>10–20 mm/yr), large fault offsets (100s km) (Tapponnier et al., 1982; Avouac and Tapponnier, 1993), the presence of zipper thrusts at the western end of the left-slip faults (Peltzer and Tapponnier, 1988; Cheng et al., 2015), and a conjugate and coeval right-slip fault with a similar slip magnitude to assist eastward lateral extrusion (scenario 1 in Fig. 3**a**). In contrast, the transfer-fault model predicts transpressional deformation at the termination thrusts oriented obliquely to the strike-slip faults (scenario 2 in Fig. 3**a**). Finally, the bookshelf fault model predicts clockwise rotation of both the left-slip faults and the fault-bounded wallrock. If the bookshelf panels are rigid, the model predicts the formation of "gaps" and/or "overlaps" at the end of the rotating blocks (scenario 3 in Fig. 3**a**); these gaps and overlaps can be reconciled

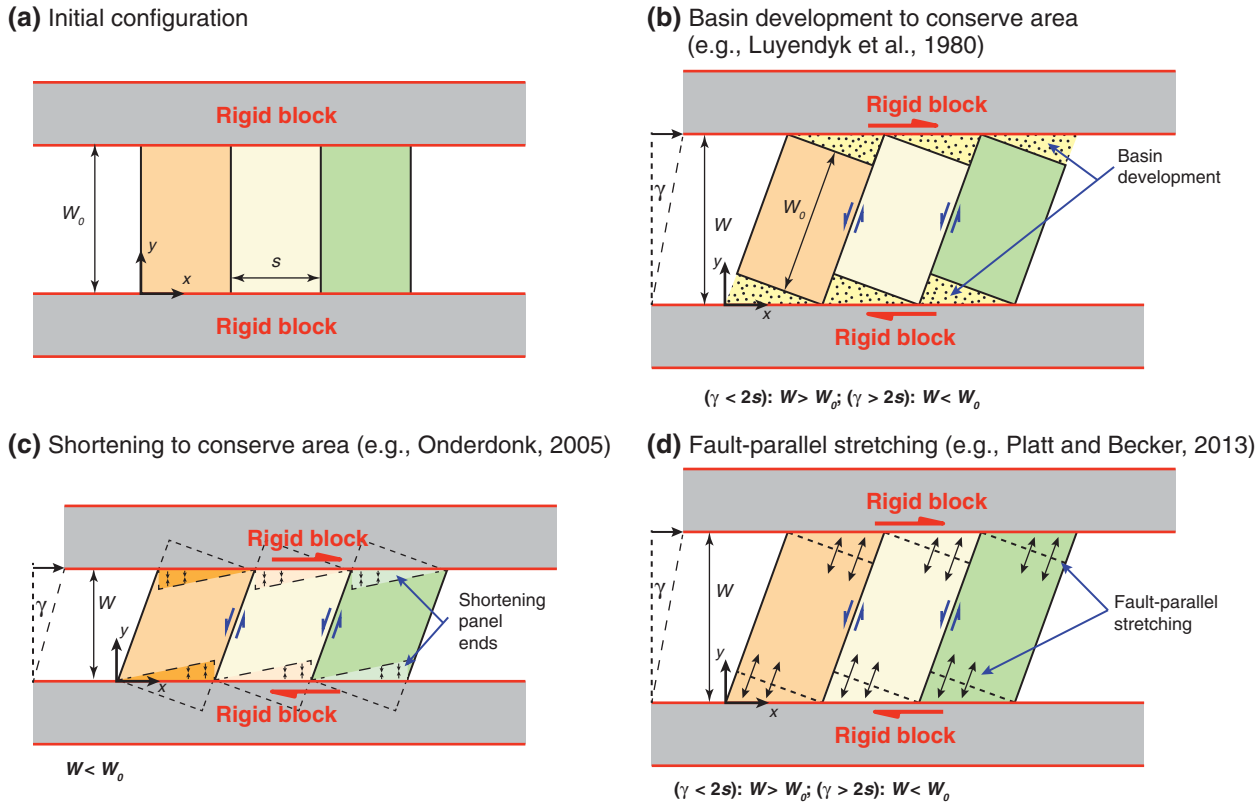

Fig 2. Conceptual models for the space issue that arises in a bookshelf fault system given an (**a**) initial configuration with three bookshelf panels bounded on the bottom and top with rigid but movable blocks. Three mechanisms have been proposed to conserve area at the ends of the panels, including (**b**) lithospheric-scale basin development (e.g., Luyendyk et al., 1980), (**c**) crustal shortening at the ends of the panels (e.g., Onderdonk, 2005), and (**d**) fault-parallel stretching throughout the panels (e.g., Platt and Becker, 2013). Note that in each case, the width of the system (W) is not constant.

by fault-parallel extension and/or shortening with non-rigid off-fault deformation (scenario 4 in Fig. 3**a**). Proposed solutions to the space issues of rigid bookshelf faulting (scenario 3 in Fig. 3**a**) include (1) extension leading to basin formation (Luyendyk et al., 1980) (Fig. 2**b**), (2) shortening within the terminal regions of the rotated blocks (e.g., Onderdonk, 2005) (Fig. 2**c**), or (3) fault-parallel stretching across the rotated blocks (e.g., Platt and Becker, 2010, 2013) (Fig. 2**d**).

2.1. Initiation age and along-strike variation of fault offsets and slip rates

A summary of inferred fault initiation ages across northern Tibet is shown in Fig. 3**b** (Yuan et al., 2013). The Haiyuan fault, which initiated at ~17–12 Ma in the west (Duvall et al., 2013) and ~8 Ma in the east (Zheng et al., 2006; Yuan et al., 2013) (Fig. 3**b**), is estimated to have 95 ± 15 km left-lateral offset at the center (Gaudemer et al., 1995) and 10–15 km slip at the eastern end (Burchfiel et al., 1991; Zhang et al., 1991) (Fig. 1). Slip along the range-bounding thrusts at the western termination of the Haiyuan fault is ≤10 km (Reith, 2013; Zuza et al., 2014, 2016) (Fig. 1), requiring a significant decrease in fault slip from the center to the western end. The bidirectional decrease in the total fault offset along the Haiyuan fault correlates with the along-fault variation of Quaternary and global positional system (GPS) velocity-field-based slip rates: 11–19 mm/yr at the center (Gaudemer et al., 1995; Lasserre et al., 1999, 2002), <5 mm/yr in the east (Zhang et al., 1991; Cavalié et al., 2008; Li et al., 2009), and 2–4 mm/yr in the west (Duvall and Clark, 2010).

The western segment of the Qinling fault is a transpressional structure that initiated at ~50 Ma (Duvall et al., 2013; Yuan et al., 2013) (Fig. 3**b**), whereas the eastern segment of the Qinling fault is a transtensional structure initiated in the Eocene with accelerated motion in the late Miocene (Mercier et al., 2013) (Fig. 1). Slip along the central and eastern sections of the Qinling fault is 20–30 km (Ratschbacher et al., 2003) with a Quaternary slip rate of 7.2 ± 2.2 mm/yr (Zhang et al., 1995). The total fault offset in the west is constrained by east–west shortening magnitude estimates of 10–15 km across both the Jishi Shan and Liupan Shan thrust belts (Fig. 1) (Zhang et al., 1991; Burchfiel et al., 1991; Lease et al., 2012). The Jishi Shan and Liupan Shan thrust belts initiated at ~13 Ma and ~8 Ma respectively (Zheng et al., 2006; Godard et al., 2009; Lease et al., 2012), corresponding to an average slip rate on the western Qinling fault of about 1–1.5 mm/yr. This is significantly less than that of the central and eastern fault segments.

The Kunlun fault initiated diachronously at 35–30 Ma in the west (Mock et al., 1999; Jolivet et al., 2003; Clark et al., 2010), 20–15 Ma along its central segment (Yuan et al., 2006; Duvall et al., 2013), and ~8 Ma in the east (Duvall et al., 2013) (Fig. 3**b**). Offset along the fault decreases bidirectionally from ~120 km in the center (Kidd and Molnar, 1988) to <10s of km at the eastern and western ends when it links with minor dip-slip fault systems (Jolivet et al., 2003; Fu and Awata, 2007) (Fig. 1). Quaternary slip rates along the central Kunlun fault of 10–12 mm/yr (Van der Woerd et al., 1998, 2000, 2002; Fu et al., 2005; Li et al., 2005) decrease to <2 mm/yr along the eastern segment (Kirby et al., 2007; Harkins and Kirby, 2008; Harkins et al., 2010). Given the fault initiation age of 35–30 Ma in the west and 20–30 km of slip along the fault (Mock et al., 1999; Jolivet et al., 2003), the average slip rate of the Kunlun fault in the west is also <2 mm/yr. Thus, slip rates along the Kunlun fault must decrease bidirectionally from the center.

These east-striking left-slip faults terminate in the west at the northwest-trending Qilian Shan-Nan Shan, Qaidam Basin, and Qimen Tagh thrust belts and in the east at the north-trending Liupan Shan and Longmen Shan thrust belts (Fig. 1). Thrusting first started at ~50 Ma in the southern Qilian Shan and northern Qaidam Basin thrust

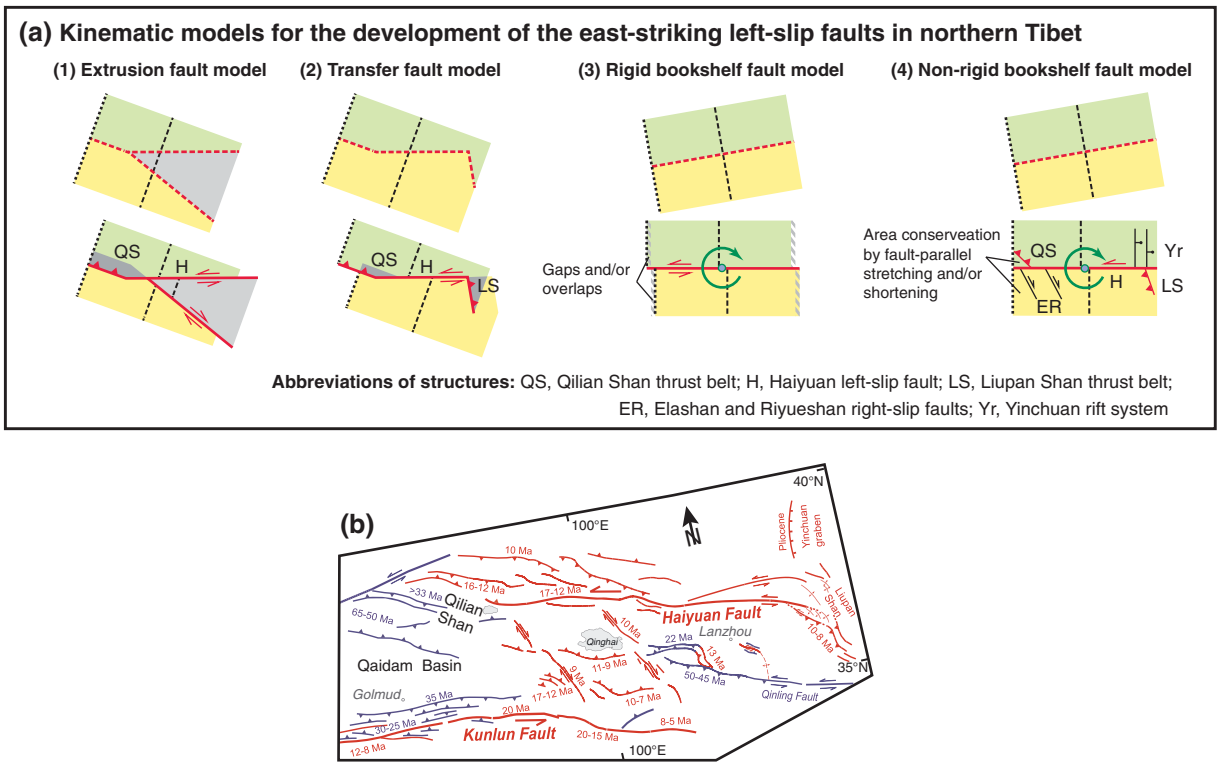

Fig. 3. (**a**) Simplified sketches showing end-member models for the role of the east-striking left-slip faults (i.e., the Haiyuan, Qinling, and Kunlun faults) in the Cenozoic tectonic development of northern Tibet. Only one left-slip fault is shown in each scenario but the same model predictions apply to each of left-slip faults in northern Tibet. Annotations show, as an example, how predicted structures match the geology for Haiyun fault and linked termination structures. The (1) extrusion fault model (e.g., Tapponnier et al., 1982) predicts the presence of a conjugate right-slip fault with a similar slip magnitude near the western end the fault, the (2) transfer fault model (e.g., Burchfiel et al., 1991; Duvall and Clark, 2010) requires a left-slip component across the termination thrusts, the (3) rigid bookshelf fault model (e.g., England and Molnar, 1990) predicts gaps and/or overlaps at the ends of the rigid blocks, and the (4) non-rigid bookshelf fault model predicts fault-parallel stretching and/or shortening to preserve mass at the panel ends (this study). (**b**) Ages of deformation in northern Tibet from numerous sources. Ages represent initiation of fault activity. Faults initiated in the Paleogene are in blue whereas faults initiated in the Neogene are red. Modified from Yuan et al. (2013). (For interpretation of the references to color in this figure legend, the reader is referred to the web version of this article.)

systems, which was followed by activity in the Qimen Tagh and the northern Qilian Shan thrust belts at 25–20 Ma (e.g., Yin et al., 2008a; Duvall et al., 2013; Cheng et al., 2014) (Fig. 3**b**). The Longmen Shan thrust belt, which involves dip-slip thrusting and minor right-slip faulting (Densmore et al., 2007; Yin, 2010b), began to develop at 30–25 Ma and accelerated deformation occurred at 15–10 Ma (Godard et al., 2009; Wang et al., 2012). The Liupan Shan thrust belt initiated at ~8 Ma (Zheng et al., 2006). Existing studies indicate a north–south shortening magnitude of 200–450 km across the three northwest-trending thrust belts (i.e., the Qimen Tagh, Qaidam Basin, and Qilian Shan-Nan Shan) (Gaudemer et al., 1995; Meyer et al., 1998; Yin et al., 2007; Yin et al., 2008a, 2008b; Gao et al., 2013; Cheng et al., 2014; Zuza et al., 2016), which contrasts sharply to the 10–40 km of shortening across the north-trending Liupan Shan and Longmen Shan thrust belts (Fig. 1) (Zhang et al., 1991; Burchfiel et al., 1995; Hubbard and Shaw, 2009).

The major left-slip faults in northern Tibet also link with extensional zones and right-slip faults (Fig. 1). The Haiyuan fault merges with the north-trending Yinchuan rift system in the east and southeast-striking right-slip Elashan and Riyueshan faults in the west (e.g., Zhang et al., 1998), the Qinling fault links with the Shanxi rift system in the east and right-slip Riyueshan-Gonghe fault in the west (e.g., Zhang et al., 1998), and the Kunlun fault links with central Tibetan rifts in the west (Yin, 2000) and the right-slip Elashan and Gonghe faults along its eastern segment (Fig. 1). Note that both the obliquely oriented western thrust belts and right-slip faults and the orthogonally oriented rifts and eastern thrust belts accommodate stretching and shortening parallel to the east-striking left-slip faults (Fig. 1). This off-fault strain pattern is inconsistent with the extrusion and transfer-fault models for the tectonic development of left-slip faulting in northern Tibet (scenarios 1 and 2 in Fig. 3**a**).

2.2. Protracted regional clockwise rotation of northern Tibet

The restoration of a series of balanced cross sections indicates an eastward decrease in north–south Cenozoic shortening across the Qaidam Basin thrust belt (Yin et al., 2008a, 2008b). A similar eastward decrease in Cenozoic shortening strain may be inferred across the Qilian Shan–Nan Shan and Qimen Tagh thrust belts on the basis of an eastward decrease in the (1) number of thrusts, (2) thrust belt width, and (3) average elevation assuming all thrusts initiated at the same elevation and have experienced the same amount of erosion (Fig. 1). The eastward decrease in shortening strain implies clockwise rotation across northern Tibet throughout much of the Cenozoic (i.e., since thrust initiation at 50–45 Ma). This observation is consistent with paleomagnetic data that suggests 15°–20° total clockwise rotation across northern Tibet with respect to the Eurasian reference pole since the Cretaceous (Fig. 4**b**) at a rate of 0.3 to 0.5°/Ma (Frost et al., 1995; Halim et al., 1998, 2003; Cogné et al., 1999; Dupont-Nivet et al., 2004; Chen et al., 2002a, 2002b; Sun et al., 2006). Variability in rotation magnitudes, ranging from 0° to >20° across the region, results from heterogeneous Cenozoic deformation (Yin et al., 2008a).

Geodetic measurements (Gan et al., 2007) show clockwise rotation of northern Tibet about an Euler pole located ~500 km to the southeast of the Eastern Himalayan Syntaxis (Fig. 4). Other workers have placed the rotation poles for northern Tibet in the western South China Sea (Peltzer and Saucier, 1996) and southwest China (Thatcher, 2007) to fit

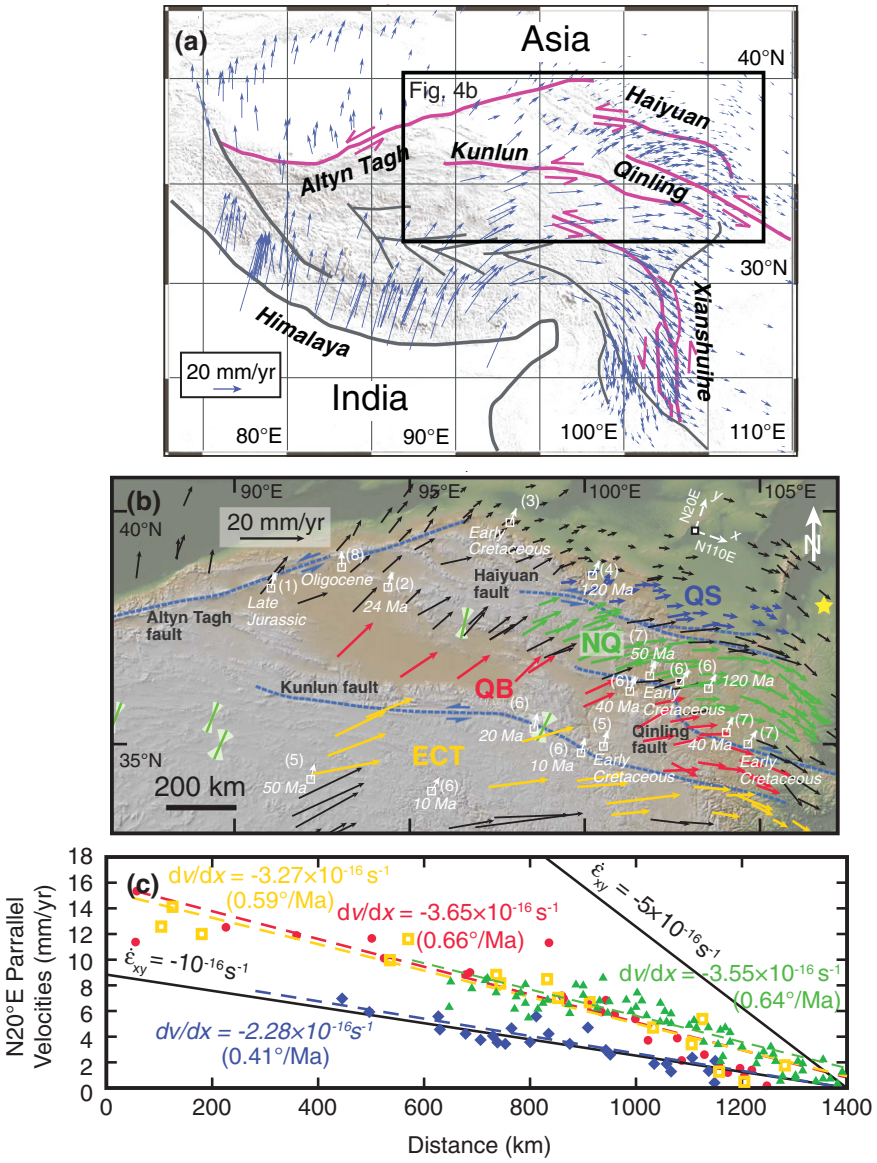

Fig. 4. (**a**) Global positioning system (GPS) velocity field across Tibet relative to stable Eurasia modified from Gan et al. (2007). Also shown is the location of Fig. 4**b**. (**b**) GPS velocity field relative to stable Eurasia with data from Gan et al. (2007). Colored vectors represent stations from four distinct domains that are bounded by the left-slip Kunlun, Qinling, and Haiyuan faults, from south to north: East Central Tibet (ECT), Qaidam Basin (QB), North Qaidam (NQ), and Qilian Shan (QS). Paleomagnetic rotation magnitudes are shown with white arrows along with the lower age bound for the onset of rotation. The averaged maximum compressive stress directions from the World Stress Map are plotted as green lines (Heidbach et al., 2008). Gold star shows the reference location for analyses in Fig. 4**c**. Also shown is the *x*–*y* coordinate system, with the *x*-axis parallel to N110°E. Paleomagnetic rotation data are from (1) Halim et al. (2003), (2) Chen et al. (2002a), (3) Chen et al. (2002b), (4) Frost et al. (1995), (5) Halim et al. (1998), (6) Cogné et al. (1999), (7) Dupont-Nivet et al. (2004), and (8) Dupont-Nivet et al. (2002). (**c**) GPS velocity component in the N20°E direction perpendicular to the general strike of the left-slip Kunlun, Qinling, and Haiyuan faults in northern Tibet. The N20°E velocity components relative to a fixed point in the Tibetan Plateau foreland (i.e., gold star in Fig. 4**b**) in each fault-bounded domain (color codes corresponding to those in Fig. 4**b**) are projected onto a N110°E-trending line. Best-fit (blue, yellow and red dashed lines) velocity gradients are bounded by shear strain rates ($\dot{\varepsilon}_{xy}$) of 10^{-16} s^{-1} and 5×10^{-16} s^{-1} shown as thick black lines. (For interpretation of the references to color in this figure legend, the reader is referred to the web version of this article.)

the global positional system (GPS) data with clockwise rotation rates of 0.5 to 1°/Ma.

We examine the velocity field across the region using the published GPS data of Gan et al. (2007) to constrain the rotation rates of the east-striking left-slip faults in northern Tibet. With this data, we derive the relative rotation and shear strain rates for four fault-bounded domains: the Qilian Shan (QS), North Qaidam (NQ), Qaidam Basin (QB), and East Central Tibet (ECT). The rotation rates of the above fault-bounded domains may approximate the fault rotation rates if present-day fault-perpendicular shortening and extension are negligible. Using the northern foreland of the Tibetan Plateau in the North China craton as a fixed reference frame (i.e., the star in Fig. 4**b**), we project fault-perpendicular velocities (i.e., N20°E, referred to as the *y*-direction) of each fault-bounded domain onto a line trending N110°E (referred to as the *x*-direction) that approximates the strike-slip fault strike (Fig. 4**b**). Note that we only picked stations that are to the north or south of the major left-slip faults (e.g., stations in the North Qaidam thrust belt were excluded) and are located more than ~50 km from the active strike-slip faults to avoid complications due to elastic behavior along locked faults. Each domain displays a relatively linear east–west velocity gradient, shear strain rate ($\dot{\gamma} = 2\dot{\varepsilon}_{xy}$), and rotation rate ($\dot{\omega}$) (Fig. 4**c**). Clockwise rotation rates are similar for the East Central Tibet, Qaidam Basin, and North Qaidam domains (i.e., 0.59°/Ma, 0.66°/Ma, and 0.64°/Ma, respectively) and decrease to 0.41°/Ma for the Qilian Shan domain in the north (Fig. 4**c**). The decrease in rotation rate across the Qilian Shan implies that central and northern Tibet are rotating in a clockwise

sense relative to North China. The magnitudes of north–south right-lateral shear strain rates ($\dot{\varepsilon}_{xy}$) vary between 1.0×10^{-16} s^{-1} and ~ 2.5×10^{-16} s^{-1} (Fig. 4**c**). These present-day rotation rates are similar with those that are geologically and paleomagnetically derived (see above), although less than then 1–2°/Ma estimated by England and Molnar (1990).

2.3. Extension and shortening within fault-bounded domains

The wallrock of the major left-slip faults, defined as the crust bounded by the strike-slip faults, displays a distinctive four-quadrant strain distribution (Fig. 5). Each strike-slip fault can be divided into four quadrants that alternate between domains of fault-parallel stretching and domains fault-parallel shortening (Fig. 5**a**). The northern wallrock of the Haiyuan fault experiences fault-parallel shortening through thrusting across the obliquely oriented Qilian Shan-Nan Shan thrust belt in the west and fault-parallel extension across the orthogonally oriented Yinchuan rift in the east (Figs. 1 and 5**b**). The southern wallrock of the Haiyuan fault experiences fault-parallel stretching via right-slip faulting in the west and fault-parallel shortening across the Liupan Shan thrust belt in the east (Figs. 1 and 5**b**). The northern and southern wallrock panels of the Qinling fault are dominated by fault-parallel contraction across the Jishi Shan and Liupan Shan thrust belts in the northwest and a contractional zone bounding the southeastern edges of the Qinling and Daba Shan in the east (Figs. 1 and 5). In contrast, the Qinling wallrock is characterized by fault-parallel extension along the Shanxi rift system to the northeast and a right-slip fault system to the southwest (Fig. 5**b**). The Kunlun fault also displays a four-quadrant deformation pattern expressed by shortening across the Qimen Tagh and Min Shan-Longmen Shan thrust belts and extension across north-striking Tibetan rifts and right-slip faulting (Kirby et al., 2000; Jolivet et al., 2003; Wang and Burchfiel, 2004; Yin et al., 2007, 2008b; Duvall and Clark, 2010; Cheng et al., 2014) (Fig. 5**b**).

The southeast-striking right-slip Elashan, Riyueshan and Gonghe faults may represent a secondary bookshelf faults within this larger bookshelf fault system (e.g., Duvall and Clark, 2010) (Figs. 1 and 5**b**). The fault geometries and right-slip kinematics, consistent with left-

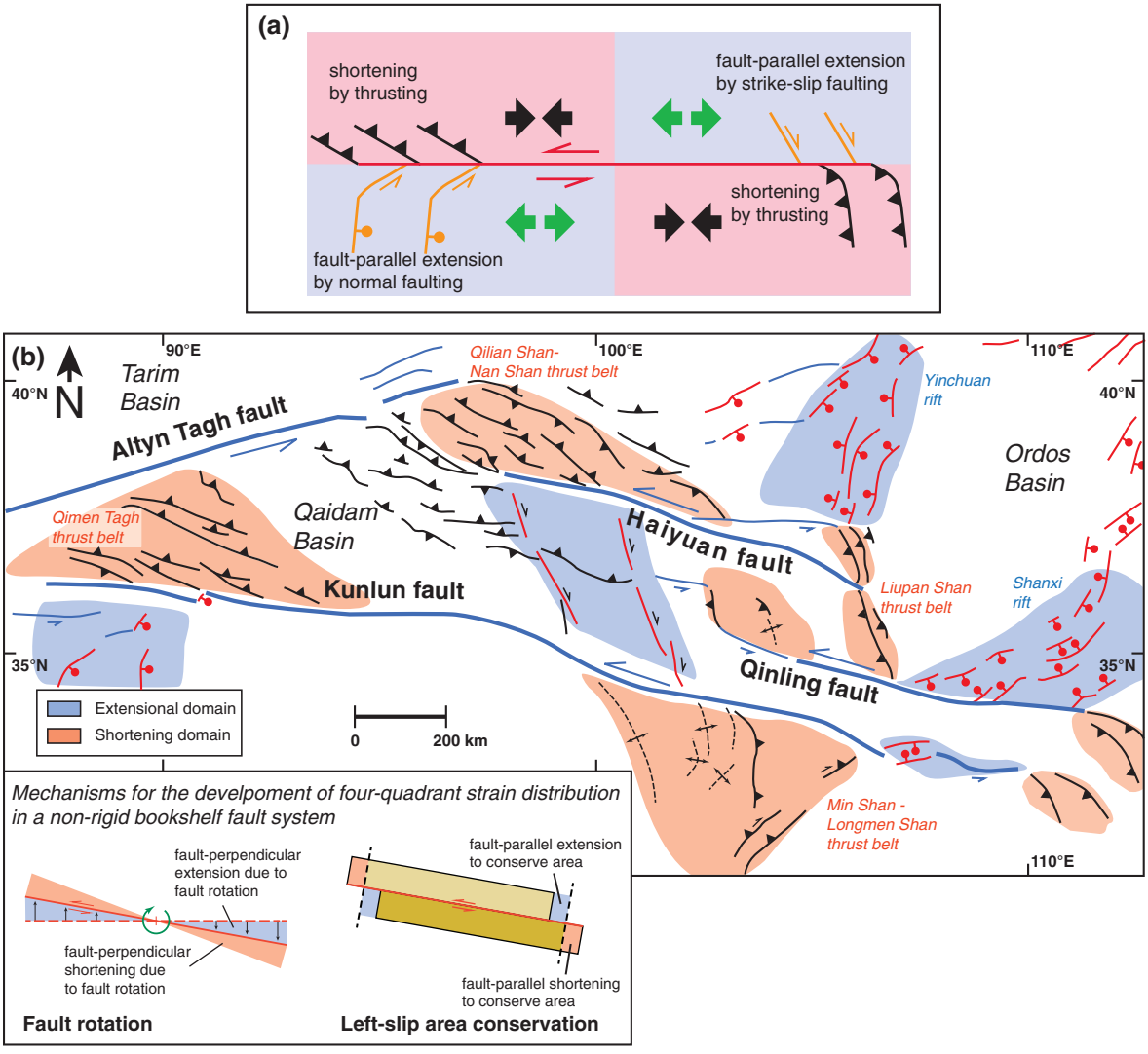

Fig. 5. (**a**) Simplified diagram highlighting a possible four-quadrant deformation pattern with a strike-slip fault and its coeval termination structures. Note that fault-parallel extension can be accommodated by either normal or strike-slip faulting. (**b**) Sketch map highlighting the relationship between east-striking left-slip faults and off-fault wallrock deformation. The Haiyuan, Qinling, and Kunlun faults all display a four-quadrant strain distribution, with fault-parallel shortening in the northwest and southeast quadrants and fault-parallel extension in the southwest and northeast quadrants. Inset shows how the non-rigid bookshelf faulting can generate the observed four-quadrant strain distribution. Fault-perpendicular deformation accommodates clockwise rotation of the faults whereas fault-parallel deformation is required to resolve the "gap" and "overlap" issues that arise at the panel ends. Note that the specific strain asymmetry corresponds to a clockwise fault rotation direction.

slip shear between the Kunlun and Haiyuan faults, also suggest north–south shortening and east–west stretching (i.e., strike-slip fault-parallel extension and fault-perpendicular shortening).

3. Non-rigid bookshelf fault model

As summarized above, existing work across northern Tibet indicates: (1) an eastward decrease in Cenozoic north–south shortening accompanied by clockwise rotation of the east-striking left-slip faults and their wallrock since the Eocene, (2) a bilateral decrease in strike-slip fault offset and slip rate along the left-slip faults that eventually almost disappears at the fault ends, and (3) a distinctive four-quadrant strain pattern in the wallrock of these faults. These observations can be tested against the existing models for the role of strike-slip faulting in accommodating India–Eurasia convergence across northern Tibet (Fig. 3**a**). The observed fault rotation is not explicitly required by the extrusion-fault and transfer-fault models (scenarios 1 and 2 in Fig. 3**a**), and neither of these models predict a four-quadrant strain pattern along the left-slip faults (Fig. 5). The observed bidirectional decrease in fault slip is also inconsistent with these models. The extrusion-fault model (scenario 1 in Fig. 3**a**) requires conjugate faults with comparable slip magnitudes, which is not observed in northern or central Tibet (Fig. 1) (cf. Cheng et al., 2015). Lastly, dip-slip north–south shortening in the western Qilian Shan-Nan Shan thrust belt near the western end of the Haiyuan fault, as indicated by fault plane solutions (Fig. 1) (e.g., Taylor and Yin, 2009) and field observations (Yin et al., 2008a; Reith, 2013; Zuza et al., 2014), is inconsistent with the transfer fault model that predicts left-slip transpression across this termination thrust system (scenario 2 in Fig. 3**a**).

At face value, the observations from northern Tibet may best be explained by a rotated-fault model. The rigid bookshelf-fault model (England and Molnar, 1990) (scenario 3 in Fig. 3**a**), based on the classic work on bookshelf faulting by Freund (1970), does not account for off-fault deformation and fails to quantify the relationship between strike-slip and dip-slip faulting. Below we propose a new non-rigid bookshelf-fault model for the development of linked left-slip faults and eastward-tapering thrust belts in northern Tibet.

3.1. Active and passive bookshelf faulting

Traditionally, the sense of shear within a bookshelf fault system is opposite that of the bounding shear zone that drives bookshelf panel rotation (Freund, 1970). For example, a left-slip bookshelf fault system requires a right-slip bounding shear zone to drive clockwise panel rotation. In this case, right-lateral shear "drags" the fault-bounded domains in a clockwise fashion. We herein refer to this process as *active* bookshelf faulting, because at least one of the bounding "walls" is moving to drive panel rotation (Fig. 6**a**). Alternatively, we introduce a new self-rotating *passive* bookshelf fault system, where the rotating panels are detached from the fixed boundary "walls" (e.g., Yin and Pappalardo, 2015) (Fig. 6**b**). In this model, the kinematics of the boundary shear zones and the individual bookshelf faults can be the same when the rotation axis is fixed in the center of the bookshelf fault system and the bounding walls are fixed (middle panel of Fig. 6**b**). Qualitatively, if the active bookshelf system is driven by drag along the edges, then the passive system is driven by a push from behind (or upward as in Fig. 6**b**) or rotation from below. Our model predicts that the top bounding surface in Fig. 6**b** absorbs shortening strain, and the magnitude of this strain varies laterally due to block rotation. Note that there are many possible variations of our passive bookshelf-fault model, depending on the relative magnitude of rigid-block rotation and rigid-block translation. For example, if the bookshelf fault system experiences both self-rotation at the panel centers and significant translation (upward in Fig. 6**b**), the sense of shear along one of the boundary shear zones may switch (bottom panel in Fig. 6**b**). Depending on the magnitude of translation, there may be little observable shear on the right boundary zone in Fig. 6**b**.

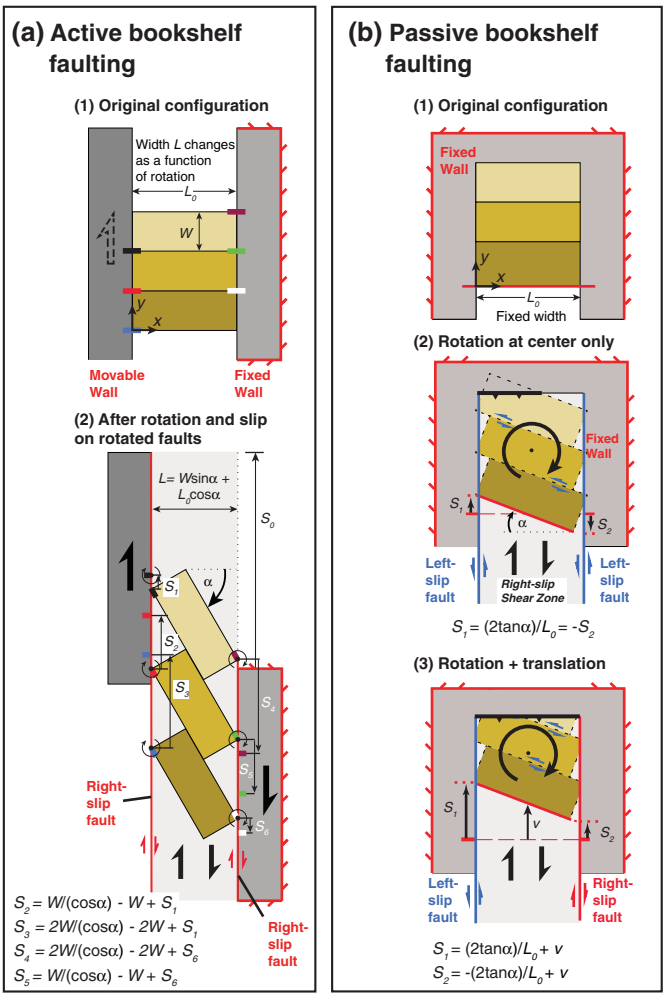

Fig. 6. (**a**) Conceptual model for the active bookshelf fault system (Freund, 1970) where shear is driven by drag along the boundary walls and the sense of shear of the bounding shear zones must be opposite of the slip between the bookshelf panels. (**b**) Conceptual model for a passive bookshelf fault system, where panels rotating about the center of the system are driven by a push from the bottom. The panels can both rotate and translate. Note that at some point between stages (2) and (3), the easternmost bounding fault transitions from left-slip to right slip, and at this point there is negligible strike-slip offset at this right-side boundary.

The geometric relationships between the initial width of the system in the *x*-direction (L_o), width of the panels in the *y*-direction (W), panel rotation magnitude (α), translation velocity magnitude (v), and boundary shear slip (e.g., S_o, S_1, S_2, etc.) are quantified, assuming rigid-body motion, in Fig. 6. For the active bookshelf fault system shown in Fig. 6**a**, translation of the left wall by S_o relative to the right wall leads to right lateral shear strain (total shear strain of S_o/L) and clockwise panel rotation (α), so that the variable width of the system (L) is

$$L = W\sin\alpha + L_o\cos\alpha \tag{1}$$

Half of the corners of the bookshelf panels remain in contact with the bounding-edge of the walls but they may slip in the *y*-direction (i.e., S_1 and S_6 in Fig. 6a), so that the system can experience more shear than the panel rotation expresses. Given that all of left-side bookshelf panel corners move relative to the left boundary wall in the *y*-direction by S_1, and $S_1 \geq 0$ (Fig. 6**a**), the slip of the other left-side corners relative to the left boundary wall is

$$S_2 = W/(\cos\alpha) - W + S_1 \tag{2a}$$

$$S_3 = 2W/(\cos\alpha) - 2W + S_1. \quad (2b)$$

Slip of the right-side corners relative to the right boundary wall is similar, except that the magnitudes are related to S_6 instead of S_1 (Fig. 6**a**).

The width of the passive bookshelf fault system remains constant ($L = L_o$) (Fig. 6**b**). Rotation of the panels in the passive bookshelf fault system of Fig. 6**b** results in boundary zone slip magnitudes (i.e., S_1 and S_2 on the left and right sides, respectively) of

$$S_1 = (2\tan\alpha)/L_o \quad (3a)$$

$$S_2 = -(2\tan\alpha)/L_o. \quad (3b)$$

Alternatively, if there is a component of translation in the y-direction (v) (bottom panel of Fig. 6**b**), the resulting boundary zone slip magnitudes are described by:

$$S_1 = (2\tan\alpha)/L_o + v \quad (4a)$$

$$S_2 = -(2\tan\alpha)/L_o + v. \quad (4b)$$

First-order deformation in either the passive or active systems can be quantified as continuous velocity fields. The idealized velocity field (i.e., no discrete faults) across an active bookshelf system is

$$u = 0 \quad (5a)$$

$$v = -\frac{v_o}{h}x \quad (5b)$$

where u and v are the velocity components in the x and y directions perpendicular and parallel to the shear zone, respectively, h is the width of the shear zone, and v_o is the velocity on one side of the shear zone at $x = -h$ relative to the other side of the shear zone (Fig. 7**a**). Note that in all of our derivations, the origin is placed at the right-side boundary, so that the left boundary is located at $x = -h$ (Fig. 7). The corresponding strain-rate-tensor components are,

$$\dot{\varepsilon}_{xx} = \frac{\partial u}{\partial x} = 0 \quad (6a)$$

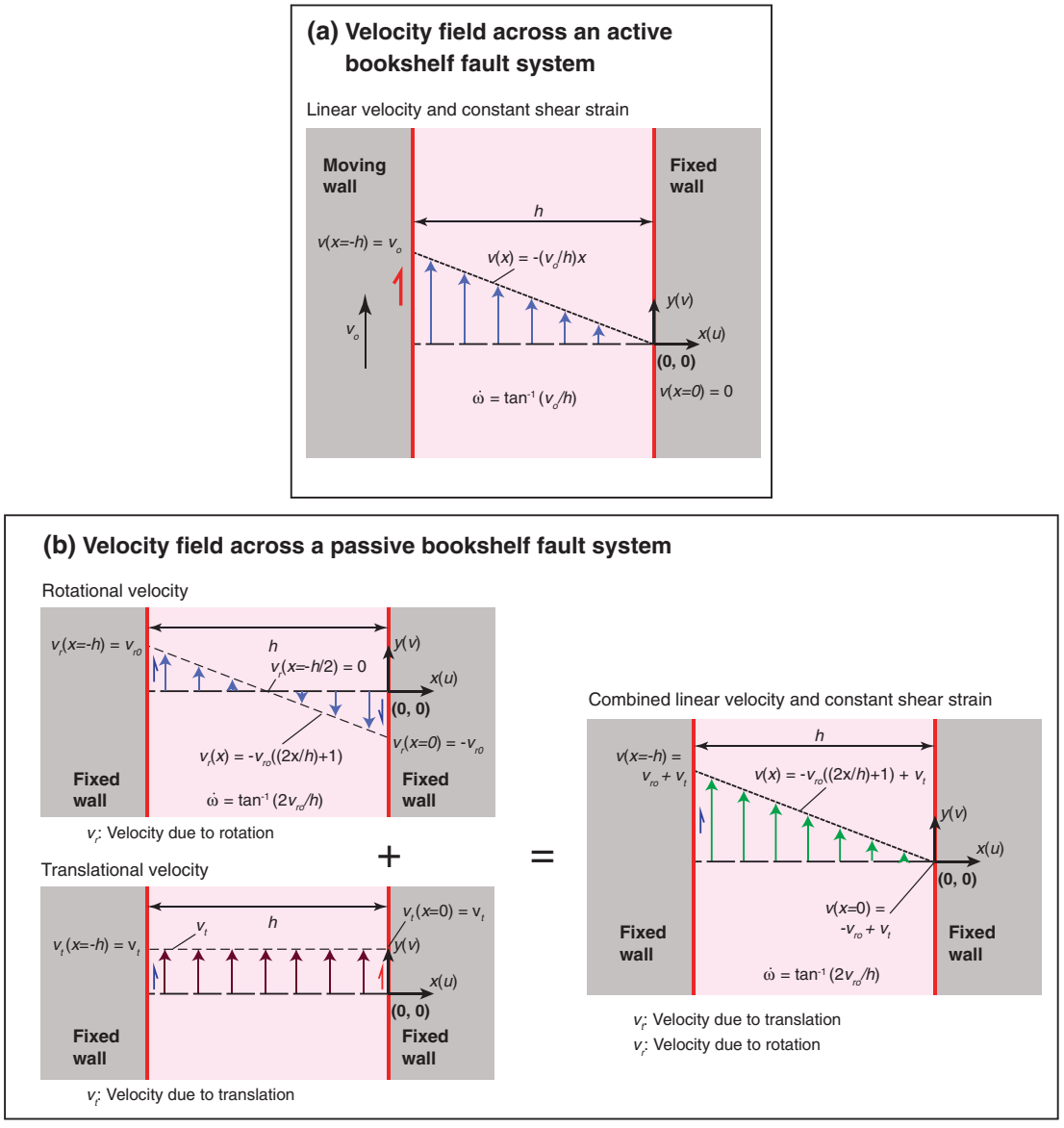

Fig. 7. Velocity fields for the (**a**) active and (**b**) passive bookshelf fault systems. Note that the velocity field in the passive system involves the summation of translational (v_t) and rotational (v_r) velocities. See text for discussion.

$$\dot{\varepsilon}_{yy} = \frac{\partial v}{\partial y} = 0 \tag{6a}$$

$$\dot{\varepsilon}_{xy} = \frac{1}{2}\left(\frac{\partial u}{\partial y} + \frac{\partial v}{\partial x}\right) = -\frac{v_o}{2h}, \tag{6c}$$

where $\dot{\varepsilon}_{xx}$ and $\dot{\varepsilon}_{yy}$ are extension strain rates in the x and y directions, perpendicular and parallel to the shear zone, and $\dot{\varepsilon}_{xy}$ is the shear strain rate (e.g., Ramsay and Huber, 1983). The rotation rate may be derived as follows:

$$\dot{\varepsilon}_{xy} = \frac{\dot{\gamma}}{2} = \frac{\tan\dot{\omega}}{2} \tag{7a}$$

$$\dot{\omega} = \tan^{-1}\frac{-v_o}{h} \tag{7b}$$

where $\dot{\omega}$ is rotation rate and $\dot{\gamma}$ is engineering or total shear strain rate (Fig. 7**a**).

Deformation for the passive bookshelf system (Fig. 7**b**) can be quantified in a similar manner, except that the velocity in the y-direction is the sum of velocities related to translation and rotation (Figs. 6**b** and 7**b**), such that

$$v = v_r + v_t \tag{8a}$$

$$v_r = -v_{ro}\left(\frac{2x}{h} + 1\right) \tag{8b}$$

$$v_t \geq 0 \tag{8c}$$

where v is the velocity component in the y-direction parallel to the shear zone, h is the width of the shear zone, v_r is velocity component related to rotation, v_{ro} is the rotation-related velocity at one side of the shear zone at $y = -h$, and v_t is the velocity component related to translation. In this approximation, we are only considering the y-component of the rotational velocity (v_r). The complete corresponding velocity field is

$$u = 0 \tag{9a}$$

$$v = -v_{ro}\left(\frac{2x}{h} + 1\right) + v_t \tag{9b}$$

where u is the velocity component in the x-direction perpendicular to the shear zone, and the other variables are the same as above (Fig. 7**b**). The strain-rate-tensor components are as follows:

$$\dot{\varepsilon}_{xx} = \frac{\partial u}{\partial x} = 0 \tag{10a}$$

$$\dot{\varepsilon}_{yy} = \frac{\partial v}{\partial y} = 0 \tag{10b}$$

$$\dot{\varepsilon}_{xy} = \frac{1}{2}\left(\frac{\partial u}{\partial y} + \frac{\partial v}{\partial x}\right) = \frac{-v_{ro}}{h} \tag{10c}$$

from which the rotation rate is given by

$$\dot{\omega} = \tan^{-1}\frac{-2v_{ro}}{h}. \tag{11}$$

3.2. Non-rigid bookshelf faulting in northern Tibet: passive and stretchy

We propose that the clockwise rotating east-striking left-slip faults in northern Tibet are part of a passive bookshelf system (Fig. 6**b**) because they are bounded to the northwest by the left-slip Altyn Tagh fault (Fig. 1). An active left-slip bookshelf fault system (Fig. 6**a**) would require a right-slip bounding shear zone to drive clockwise panel rotation, whereas the passive system allows the panels to rotate in a clockwise fashion against a rigid boundary to the west, creating a left-slip shear zone. This simple model involving clockwise rotation across the region may explain why Tibet is bounded by left-slip fault system to the northwest (i.e., the Altyn Tagh fault) and minor-to-insignificant right-slip faulting to the southeast (i.e., within the Longmen Shan) (Fig. 1), rather than the expected broad right-slip shear zones as predicted by the classic rigid-bookshelf model (England and Molnar, 1990).

The predicted velocity field from the passive bookshelf system (Eqs. (9a) and (9b)) can be compared to the GPS-derived velocity field across northern Tibet (Fig. 4). The eastern boundary of northern Tibet does not have a significant north-striking strike-slip bounding fault like the western boundary (i.e., the Altyn Tagh fault); only minor right-slip faulting is observed in the Longmen Shan (Densmore et al., 2007; Yin, 2010b) (Fig. 1). Because of this, we can infer that the N–S velocity due to clockwise rotation is matched by the northward translation velocity, so that v_{ro} is equal but opposite to v_t at $x = 0$ (the eastern boundary) (Fig. 7**b**) in Eqs. (9a) and (9b). The N20°E velocity gradient plotted in Fig. 4**c** shows a maximum velocity near the western boundary ($x = -h$) of ~16 mm/yr, which requires v_r and v_t of Eqs. (9a) and (9b) to equal ~8 mm/yr. A northward translational velocity (v_t) of 8 mm/yr is reasonable given that the northward GPS velocities just south of the Kunlun fault are 7–15 mm/yr (Zhang et al., 2004; Yin and Taylor, 2011). If we assume that the fixed width of the system h is 1400 km (Fig. 1), the N–S velocity field can be described by $v = (-1.14 \times 10^{-8})x\ \mathrm{yr}^{-1}$ (Fig. 7**b**). The resulting shear strain rate and clockwise rotation rate are $\dot{\varepsilon}_{xy} = -1.81 \times 10^{-16}\ \mathrm{s}^{-1}$ and $\dot{\omega} = 0.65°/\mathrm{Ma}$ respectively. These rates are comparable to the paleomagnetic, geologic, and geodetic data discussed above.

Since the boundary domains in the active or passive bookshelf system are relatively rigid, the bookshelf panels must be non-rigid to resolve the space issues that arise at the panel ends (Figs. 2 and 6) (e.g., Luyendyk et al., 1980; Onderdonk, 2005; Platt and Becker, 2013). The necessary fault-parallel stretching or shortening of the fault-bounded domains accommodates negligible slip at the ends of each rotating fault. The strike-slip faults in a non-rigid bookshelf system, bounded by deformable rather than rigid wallrock, are referred to as stretching faults (Means, 1989, 1990).

Unlike the models of either Onderdonk (2005) or Platt and Becker (2013), the bookshelf panels in our non-rigid passive bookshelf model do not have to either *all stretch* or *all shorten* to accommodate rotation in a deforming material. Instead, each quadrant of wallrock deforms according to the kinematics of the bounding strike-slip faults, so that off-strike-slip-fault wallrock deformation accommodates negligible slip at the strike-slip faults tips (Fig. 5). An example of a possible interaction along the left-most boundary is shown in Fig. 8. Given the small angle of clockwise rotation of the left-slip faults ($\theta \ll 1°$), the resulting left-lateral slip (d) must be accommodated by fault-parallel stretching and shortening strain (ε_{xx}) in the panels adjacent to the strike-slip fault (i.e., panels A and B in Fig. 8). Assuming that the resulting strain is homogenous throughout one-half of the bookshelf panel and affects both panels A and B by the same magnitude, this strain can be written as:

$$\varepsilon^A{}_{xx} = \frac{1}{2}\frac{d}{S} \tag{12a}$$

$$\varepsilon^B{}_{xx} = -\frac{1}{2}\frac{d}{S} \tag{12b}$$

where $\varepsilon^A{}_{xx}$ and $\varepsilon^B{}_{xx}$ are the extension strain in panel A and panel B, respectively, d is the left-lateral slip, and S is the half the length of the bookshelf panel ($S = L/2$), all in the x-direction (Fig. 8). Because this left-slip (d) is

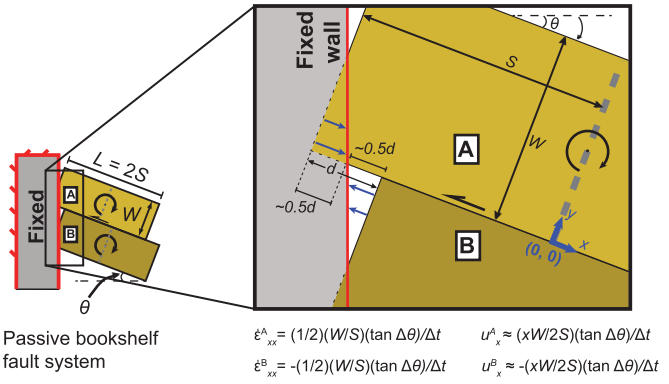

Fig. 8. Kinematic model illustrating the required fault-parallel strain at the western end of one passive bookshelf fault. Given a rigid left-side boundary, left-lateral offset on the fault (d) caused by clockwise fault rotation requires fault-parallel shortening and stretching strain (ε_{xx}), for panels A and B respectively, related to approximately one-half the fault slip divided by half the length of each panel, L: $\varepsilon^A_{xx} \approx 0.5d/L$ and $\varepsilon^B_{xx} \approx -0.5d/L$. In this example, the angle of rotation, θ, is very small, such that $\tan\theta$ can be approximated as θ. See text for discussion.

caused by clockwise rotation, we can relate this strain to rotation rate, and derive the resulting fault-parallel strain rate:

$$\dot{\varepsilon}^A{}_{xx} = \frac{1}{2}\frac{W}{S}\frac{\tan(\Delta\theta)}{\Delta t} \tag{13a}$$

$$\dot{\varepsilon}^B{}_{xx} = -\frac{1}{2}\frac{W}{S}\frac{\tan(\Delta\theta)}{\Delta t} \tag{13b}$$

where W is the width of the bookshelf panel in the y-direction, $\Delta\theta$ is the small angle of clockwise rotation of the left-slip faults over a short timescale (Δt), and the other variables are the same as above. The corresponding velocity field may be written as,

$$u^A{}_x = \frac{x}{2}\frac{W}{S}\frac{\tan(\Delta\theta)}{\Delta t} + c \tag{14a}$$

$$u^B{}_x = -\frac{x}{2}\frac{W}{S}\frac{\tan(\Delta\theta)}{\Delta t} + c \tag{14b}$$

where $u^A{}_x$ and $u^B{}_x$ are the velocity components in the x-direction in panels A and B respectively, and c is a constant of integration may be dropped by setting the boundary condition of $u_x = 0$ at $x = 0$ (Fig. 8). Combining Eqs. (14a), (14b), and (11) yields an expression for fault-parallel stretching rate (u_x) as a function of v_{ro}:

$$u^A{}_x = \frac{x}{2}\frac{W}{S}\tan^{-1}\frac{-2v_{ro}}{h} \tag{15a}$$

$$u^B{}_x = -\frac{x}{2}\frac{W}{S}\tan^{-1}\frac{-2v_{ro}}{h}. \tag{15b}$$

If we take v_{ro} to be 8 mm/yr (as discussed above), the bookshelf panel between the Kunlun and Qinling faults to have a width of 150 km and length of 1400 km ($S = 700$ km) (Fig. 1), and the width of the bookshelf system h as 1400 km, we arrive at fault-parallel stretching rates of ~1 mm/yr. For the Kunlun fault, as an example, this should be accommodated by fault-parallel shortening in the Qimen Tagh and extension to the south in central Tibet at a rate of ~1 mm/yr (Fig. 1).

4. Discussion

4.1. Driving mechanisms for clockwise rotation

Applying the passive bookshelf fault model to northern Tibet requires clockwise rotation of the left-slip faults and fault-bounded wallrock relative to the relatively fixed Tarim and North China (i.e., the top, left, and right sides of the passive bookshelf fault system in Fig. 6**b**). This system can be driven by either rotation of the bottom boundary (i.e., rotation of central and southern Tibet) or basal drag beneath the system. In the simplest case, clockwise rotation of southern Tibet and/or the Himalaya relative to North China (Fig. 9**a**) can drive clockwise rotation of northern Tibet. Due to the lack of paleomagnetic and GPS data across central and southern Tibet, this model is difficult to test with confidence (Figs. 1 and 4**a**). However, existing geologic data from central and southern Tibet suggest that the regions are actually experiencing counterclockwise rotation (e.g., Yin, 2006; Burgess et al., 2012), which is inconsistent with the model requirements.

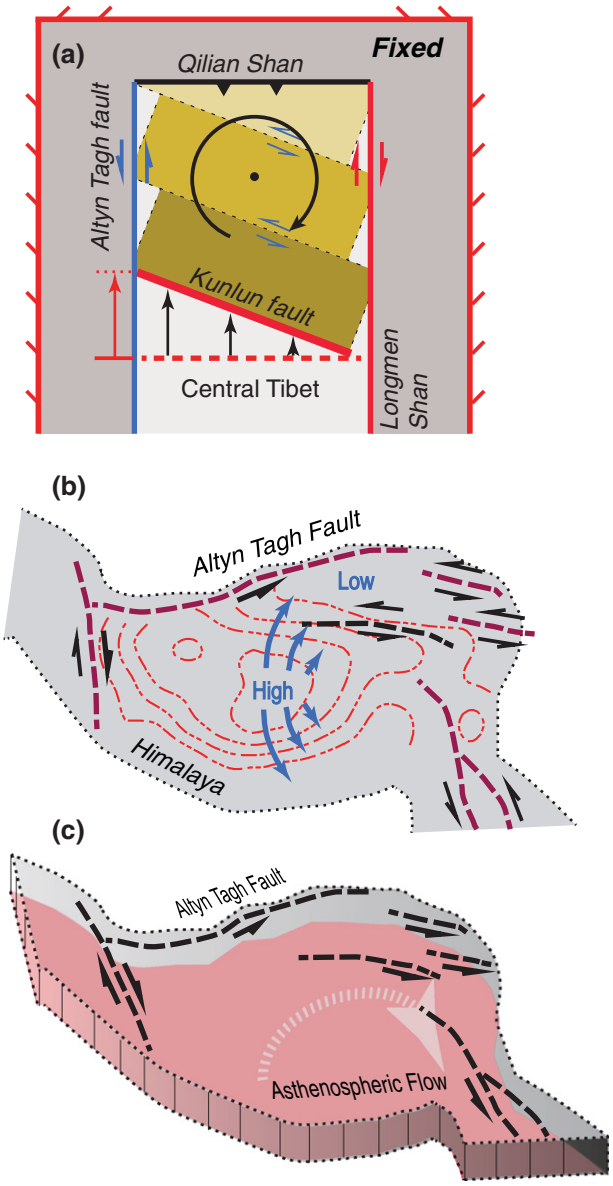

Fig. 9. Passive bookshelf faulting in northern Tibet may be driven by (**a**) boundary-zone rotation to the south, (**b**) gravitational spreading of thick central Tibet lithosphere with the distribution of gravitational potential energy after England and Molnar (1997), or (**c**) a toroidal flow in the asthenosphere (e.g., León Soto et al., 2012). See text for further discussion.

Alternatively, rotation of northern Tibet could have been driven by an eastward decrease in gravitational potential energy (GPE) and GPE gradient in central Tibet (England and Molnar, 1997) (Fig. 9**b**). This GPE distribution may lead to faster spreading of the thickened lithosphere in the west than that in the east, causing clockwise rotation of northern Tibet. One potential problem is that this model would require north–south extension across central Tibet that is not observed. However, the spreading-induced extensional strain may be overwhelmed by India-indentation-induced shortening strain in the region. It is also possible that fault rotation in northern Tibet is driven by a toroidal asthenospheric flow (Fig. 9**c**) that develops as the Burma trench, which is located just south of the Eastern Himalayan Syntaxis, retreats westward. The roll-back of the Burma slab causes poloidal flow of the asthenosphere around the slab, which draws in a toroidal flow around its northern edge. This inference is consistent with the current knowledge of mantle seismic anisotropy in the region (e.g., León Soto et al., 2012).

4.2. Implications for the Cenozoic development of northern Tibet

Recent work on the timing of structures in northern Tibet suggests a two-stage development of the region (Fig. 3**b**), with a change from thrust-dominated to strike-slip-dominated deformation at 20 to 15 Ma (e.g., Craddock et al., 2011; Duvall et al., 2013) due to a change in boundary conditions and stress regime (Yuan et al., 2013). As

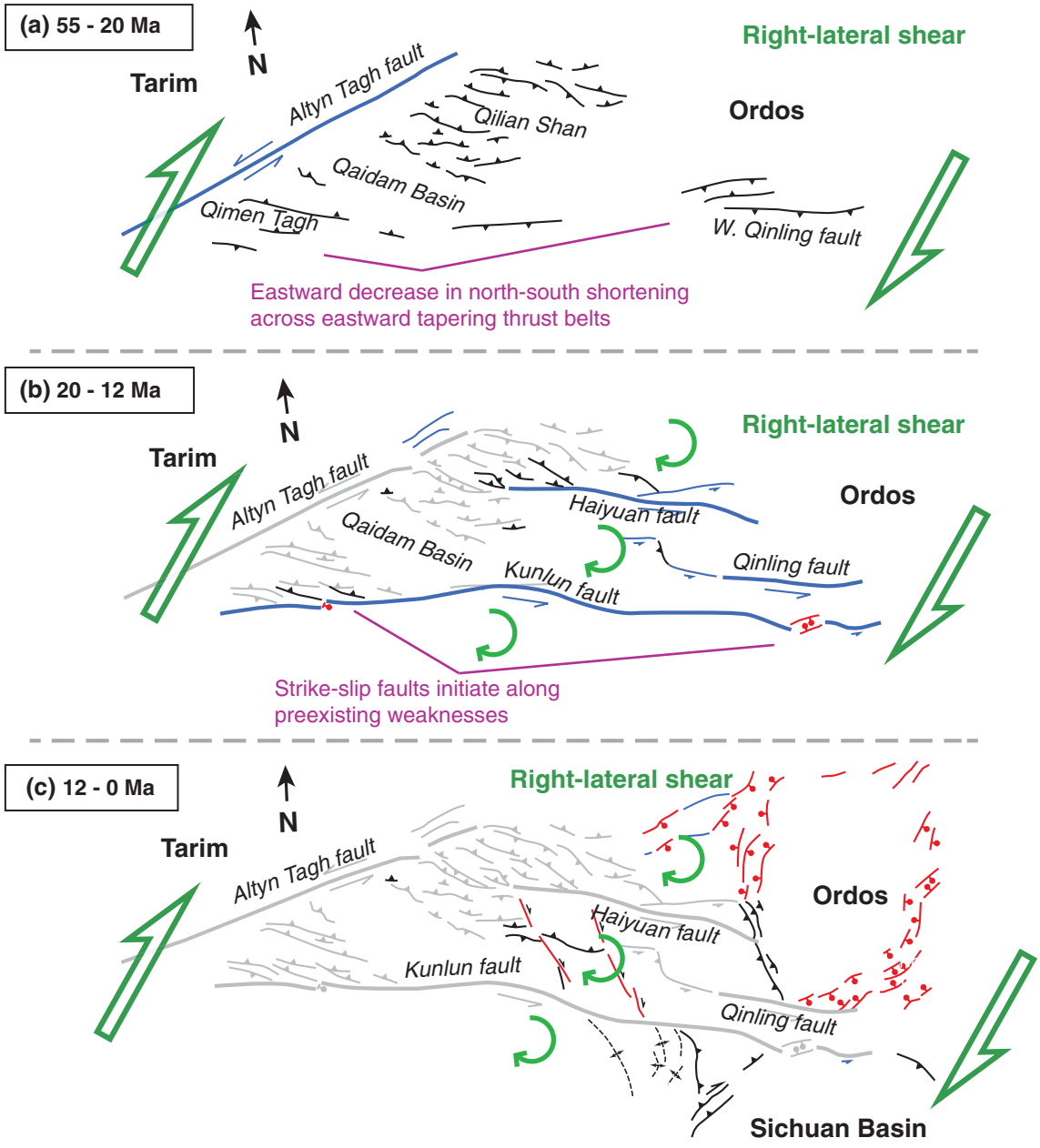

Fig. 10. Cenozoic tectonic evolution of northern Tibet, showing the timing of major fault initiation where gray structures are already active at the given time interval. Note orientation of north arrows. (**a**) Right-lateral shear, driven from the south, begins in the Eocene and is expressed by north–south shortening in the Qimen Tagh, North Qaidam, and southern Qilian Shan thrust belts. An eastward decrease in north–south shortening magnitude and thrust spacing indicates clockwise rotation of northern Tibet. (**b**) Progressive crustal thickening causes the initiation of the east-striking left-slip faults along preexisting weaknesses. Continued right-lateral shear drives clockwise rotation of these faults and their wallrock passively against the left-slip Atlyn Tagh bounding fault zone. (**c**) The left-slip faults in this passive bookshelf fault system develop a four-quadrant deformation pattern with domains of fault-parallel stretching and shortening. Age data from Craddock et al. (2011); Yuan et al. (2013); Duvall et al. (2013), and references therein.

discussed by Clark (2012), the average bulk strain rate (i.e., $\dot{\varepsilon} = v/L$) across the Himalayan–Tibetan orogen has remained constant since the onset of collision ($\dot{\varepsilon} = \sim 7 \times 10^{-16}\ s^{-1}$); deformation and narrowing of the orogen (L) has been balanced by slowed plate convergence (v) as a result of viscous mantle resistance. A constant strain for a viscous medium (i.e., the Tibetan–Eurasian lithosphere) equates to constant contractional stress acting on it, regardless of a shift in the geodynamics (e.g., crustal thickness, rheology, boundary conditions). Our calculated present-day shear strain rates and clockwise rotation rates across northern Tibet are consistent with geologic and paleomagnetic rotation rates. This similarity suggests that strain rates have remained constant throughout the Cenozoic, which is inconsistent with the discrete two-stage deformation model for the development of northern Tibet (e.g., Yuan et al., 2013) that requires a change in boundary conditions. Alternatively, the non-rigid passive bookshelf model proposed in this study implies that coeval and kinematically linked thrust and strike-slip faulting could have formed under a constant stress regime.

The fundamental mode of Cenozoic deformation in northern Tibet appears to be protracted north-trending right-lateral simple shear (England and Molnar, 1990), nearly parallel to the northeast-striking Altyn Tagh fault, since the onset (or soon after) of the India–Eurasian collision at 60–55 Ma (e.g., Zhu et al., 2005; Green et al., 2008; Dupont-Nivet et al., 2010) (Fig. 10). Right-lateral shear strain was accommodated in the Eocene–Oligocene to early Miocene by distributed shortening and crustal-thickening in the Qimen Tagh, Qaidam Basin, and southern Qilian Shan thrust belts (Fig. 10**a**). An eastward decrease in north–south shortening strain was associated with the passive clockwise rotation of northern Tibet against the left-slip Altyn Tagh fault.

Crustal thickening led to a reorientation of the intermediate compressive stress orientation from horizontal to vertical by 20 to 15 Ma that shifted deformation to a mixed-mode of thrusting and left-slip faulting along preexisting weaknesses (i.e., Phanerozoic sutures) (Fig. 10**b**). The clockwise rotation and northward translation of the east-striking left-slip Haiyuan, Qinling, and Kunlun faults against the left-slip Altyn Tagh bounding fault zone in the northwest and the Longmen Shan in the southeast operated as passive bookshelf fault system. Combined northward translation and clockwise rotation of northern Tibet lead to minor observable right-slip shear along the eastern northeast-striking bounding faults (i.e., right-slip faulting within the thrust belt) (Figs. 6**b** and 10**b**). The rotating fault-bounded domains, surrounded by a relatively rigid medium (i.e., a strong Tarim and North China) (e.g., Molnar and Tapponnier, 1981), require fault-parallel deformation to resolve the space issues at the panel ends (Fig. 10**c**). Note that the Altyn Tagh fault is oblique to the regional shear direction, and this orientation results in more shortening in the west than the east as the left-slip faults rotate against rigid Tarim and the Altyn Tagh boundary shear zone. Wallrock deformation and subsequent fault stretching (Means, 1989) result in negligible fault slip at the ends of each east-striking left-slip fault.

Several testable predictions emerge from our proposed model. First, the east-striking left-slip faults should be relatively weak. The western and central sections of the faults strike at a high angle to the maximum compressive stress direction (Fig. 4**b**) which indicates that minimal shear stress is acting on the fault planes. The faults also initiated along sutures (Fig. 1) that are presumably zones of preexisting weaknesses. The orthogonal orientation of the strike-slip faults to the maximum compressive stress direction in the west allows for the development of thrust belts that obliquely merge with the left-slip faults, as opposed to the eastern thrust belts that develop orthogonally to the strike-slip faults (Fig. 1). Second, the distinct two stages of deformation in northern Tibet (e.g., Yuan et al., 2013) may be apparent as a result of limited sampling and loose timing constraints. For example, we note that there are no direct age constraints for the initiation of the Haiyuan fault (Yuan et al., 2013) (Fig. 3**b**). The complex deformational patterns in northern Tibet make differentiating between thrust and strike-slip fault initiation difficult with current thermochronology techniques. Lastly, detailed studies of crustal strain can reveal if the fault-parallel shortening and extension in the off-fault regions equal offset on the strike-slip faults. There is currently little detailed structural data across the Qimen Tagh and Qilian Shan thrust belts to convincingly test this hypothesis, and GPS stations are sparse in these regions (Fig. 4**a**).

An important implication of the non-rigid bookshelf-fault model is that the style and magnitude of Cenozoic deformation in northern Tibet vary considerably in the east–west direction. In order to understand processes of continental deformation and plateau construction, future geologic studies must establish along-strike variations of the structural framework along the left-slip faults to examine the relationship between discrete left-slip faulting and distributed off-fault deformation. It is clear that a single north–south cross section and its kinematic reconstruction across the northeastern margin of the Tibetan Plateau would not properly quantify the complex deformational processes of plateau formation.

5. Conclusions

The Cenozoic tectonic development of northern Tibet is characterized by the clockwise rotation of three major east-striking left-slip faults. Similar rotation and shear strain rates from paleomagnetic, geologic, and geodetic datasets (e.g., $\dot{\varepsilon_{xy}} = \sim 10^{-16}\ s^{-1}$) suggest continuous clockwise rotation of the region since the Eocene, which is consistent with a constant bulk strain rate across the Himalayan–Tibetan orogen since the onset of India–Eurasia collision (Clark, 2012). Our proposed non-rigid passive bookshelf-fault model, which relates discrete left-slip faulting to distributed off-fault deformation during regional clockwise rotation, accounts for the rotation of major left-slip faults, bidirectional decrease in slip from the central segments of these faults, eastward-tapering northwest-trending thrust belts, and four-quadrant strain pattern in the wallrock of the strike-slip faults. This model quantifies the relationship between strike-slip faulting and off-fault deformation during processes of continental tectonics and highlights the complexity of Cenozoic continental deformation in northern Tibet.

Acknowledgements

An Yin's research in Tibet has been supported by grants from the Tectonics Program of the US National Science Foundation. We thank Paul Mann and an anonymous reviewer, as well as editor Jean-Philippe Avouac, for their constructive comments on the manuscript.

References

Avouac, J.P., Tapponnier, P., 1993. Kinematic model of active deformation in Central Asia. Geophys. Res. Lett. 20 (10), 895–898.
Burchfiel, B.C., Zhang, P., Wang, Y., Zhang, W., Song, F., Deng, Q., Molnar, P., Royden, L., 1991. Geology of the Haiyuan fault zone, Ningxia Hui Autonomous Region, China, and its relation to the evolution of the northeastern margin of the Tibetan Plateau. Tectonics 10, 1091–1110.
Burchfiel, B.C., Chen, Z., Liu, Y., Royden, L.H., 1995. Tectonics of the Longmen Shan and adjacent regions. Int. Geol. Rev. 661–735 (37p).
Burgess, W.P., Yin, A., Dubey, C.S., Shen, Z.K., Kelty, T.K., 2012. Holocene shortening across the main frontal thrust zone in the eastern Himalaya. Earth Planet. Sci. Lett. 357, 152–167.
Cavalié, O., Lasserre, C., Doin, M.P., Peltzer, G., Sun, J., Xu, X., Shen, Z.K., 2008. Measurement of interseismic strain across the Haiyuan fault (Gansu, China), by InSAR. Earth Planet. Sci. Lett. 275 (3), 246–257.
Chen, Y., Gilder, S., Halim, N., Cogné, J.P., Courtillot, V., 2002a. New paleomagnetic constraints on central Asian kinematics: displacement along the Altyn Tagh fault and rotation of the Qaidam Basin. Tectonics 21 (5) (p. 6-1).
Chen, Y., Wu, H., Courtillot, V., Gilder, S., 2002b. Large N–S convergence at the northern edge of the Tibetan plateau? New Early Cretaceous paleomagnetic data from Hexi Corridor, NW China. Earth Planet. Sci. Lett. 201 (2), 293–307.
Cheng, F., Jolivet, M., Fu, S., Zhang, Q., Guan, S., Yu, X., Guo, Z., 2014. Northward growth of the Qimen Tagh range: a new model accounting for the late Neogene strike-slip deformation of the SW Qaidam Basin. Tectonophysics 632, 32–47.
Cheng, F., Jolivet, M., Dupont-Nivet, G., Wang, L., Yu, X., Guo, Z., 2015. Lateral extrusion along the Altyn Tagh fault, Qilian Shan (NE Tibet): insight from a 3D crustal budget. Terra Nova 27 (6), 416–425.

Clark, M.K., 2012. Continental collision slowing due to viscous mantle lithosphere rather than topography. Nature 483 (7387), 74–77.

Clark, M.K., Farley, K.A., Zheng, D., Wang, Z., Duvall, A.R., 2010. Early Cenozoic faulting of the northern Tibetan Plateau margin from apatite (U–Th)/He ages. Earth Planet. Sci. Lett. 296 (1), 78–88.

Cobbold, P.R., Davy, P.H., 1988. Indentation tectonics in nature and experiment. 2. Central Asia. Bull. Geol. Inst. Univ. Uppsala 14, 143–162.

Cogné, J.P., Halim, N., Chen, Y., Courtillot, V., 1999. Resolving the problem of shallow magnetizations of Tertiary age in Asia: insights from paleomagnetic data from the Qiangtang, Kunlun, and Qaidam blocks (Tibet, China), and a new hypothesis: journal of geophysical research. Solid Earth 104 (B8), 17715–17734.

Craddock, W., Kirby, E., Zhang, H., 2011. Late Miocene–Pliocene range growth in the interior of the northeastern Tibetan Plateau. Lithosphere 3 (6), 420–438.

Densmore, A.L., Ellis, M.A., Li, Y., Zhou, R., Hancock, G.S., Richardson, N., 2007. Active tectonics of the Beichuan and Pengguan faults at the eastern margin of the Tibetan Plateau. Tectonics 26 (4).

Dupont-Nivet, G., Guo, Z., Butler, R.F., Jia, C., 2002. Discordant paleomagnetic direction in Miocene rocks from the central Tarim Basin: evidence for local deformation and inclination shallowing. Earth Planet. Sci. Lett. 199 (3), 473–482.

Dupont-Nivet, G., Horton, B.K., Butler, R.F., Wang, J., Zhou, J., Waanders, G.L., 2004. Paleogene clockwise tectonic rotation of the Xining-Lanzhou region, northeastern Tibetan Plateau. J. Geophys. Res. 109. http://dx.doi.org/10.1029/2003JB002620.

Dupont-Nivet, G., Lippert, P.C., Van Hinsbergen, D.J., Meijers, M.J., Kapp, P., 2010. Palaeolatitude and age of the Indo-Asia collision: palaeomagnetic constraints. Geophys. J. Int. 182 (3), 1189–1198.

Duvall, A.R., Clark, M.K., 2010. Dissipation of fast strike-slip faulting within and beyond northeastern Tibet. Geology 38, 223–226.

Duvall, A.R., Clark, M.K., Kirby, E., Farley, K.A., Craddock, W.H., Li, C., Yuan, D.Y., 2013. Low-temperature thermochronometry along the Kunlun and Haiyuan faults, NE Tibetan Plateau: evidence for kinematic change during late-stage orogenesis. Tectonics 32 (5), 1190–1211.

England, P., Houseman, G., 1986. Finite strain calculations of continental deformation: 2. Comparison with the India–Asia collision zone: journal of geophysical research. Solid Earth 91 (B3), 3664–3676.

England, P., Molnar, P., 1990. Right-lateral shear and rotation as the explanation for strike-slip faulting in eastern Tibet. Nature 344, 140–142.

England, P., Molnar, P., 1997. Active deformation of Asia: from kinematics to dynamics. Science 278, 647–650.

Freund, R., 1970. Rotation of strike slip faults in Sistan, southeast Iran. J. Geol. 78, 188–200.

Frost, G.M., et al., 1995. Preliminary early Cretaceous paleomagnetic results from the Gansu Corridor, China. Earth Planet. Sci. Lett. 129 (1), 217–232.

Fu, B., Awata, Y., 2007. Displacement and timing of left-lateral faulting in the Kunlun fault zone, northern Tibet, inferred from geologic and geomorphic features. J. Asian Earth Sci. 29, 253–265.

Fu, B., Awata, Y., Du, J., He, W., 2005. Late Quaternary systematic stream offsets caused by repeated large seismic events along the Kunlun fault, northern Tibet. Geomorphology 71 (3), 278–292.

Gan, W., Zhang, P., Shen, Z.-K., Niu, Z., Wang, M., Wan, Y., Zhou, D., Cheng, J., 2007. Present-day crustal motion within the Tibetan Plateau inferred from GPS measurements. J. Geophys. Res. 112 (B8).

Gao, R., Wang, H., Yin, A., Dong, S., Kuang, Z., Zuza, A.V., Li, W., Xiong, X., 2013. Tectonic development of the northeastern Tibetan Plateau as constrained by high-resolution deep seismic-reflection data. Lithosphere 5 (6), 555–574.

Gaudemer, Y., Tapponnier, P., Meyer, B., Peltzer, G., Guo, S., Chen, Z., Dai, H., Cifuentes, I., 1995. Partitioning of crustal slip between linked, active faults in the eastern Qilian Shan, and evidence for a major seismic gap, the 'Tianzhu gap', on the western Haiyuan fault, Gansu (China). Geophys. J. Int. 120, 599–645.

Godard, V., Pik, R., Lavé, J., Cattin, R., Tibari, B., De Sigoyer, J., Pubellier, M., Zhu, J., 2009. Late Cenozoic evolution of the central Longmen Shan, eastern Tibet: insight from (U-Th)/He thermochronometry. Tectonics 28 (5).

Green, O.R., Searle, M.P., Corfield, R.I., Corfield, R.M., 2008. Cretaceous–Tertiary carbonate platform evolution and the age of the India-Asia collision along the Ladakh Himalaya (Northwest India). J. Geol. 116 (4), 331–353.

Halim, N., et al., 1998. New Cretaceous and Early Tertiary paleomagnetic results from Xining-Lanzhou basin, Kunlun and Qiangtang blocks, China: implications on the geodynamic evolution of Asia. J. Geophys. Res. Solid Earth 103 (B9), 21025–21045.

Halim, N., Chen, Y., Cogné, J.P., 2003. A first palaeomagnetic study of Jurassic formations from the Qaidam basin, Northeastern Tibet, China—tectonic implications. Geophys. J. Int. 153 (1), 20–26.

Harkins, N., Kirby, E., 2008. Fluvial terrace riser degradation and determination of slip rates on strike-slip faults: an example from the Kunlun fault, China. Geophys. Res. Lett. 35 (5).

Harkins, N., Kirby, E., Shi, X., Wang, E., Burbank, D., Chun, F., 2010. Millennial slip rates along the eastern Kunlun fault: implications for the dynamics of intracontinental deformation in Asia. Lithosphere 2, 247–266.

Heidbach, O., Tingay, M., Barth, A., Reinecker, J., Kurfeß, D., Müller, B., 2008. Global crustal stress pattern based on the World Stress Map database release. Tectonophysics 482 (1), 3–15 (2010).

Hubbard, J., Shaw, J.H., 2009. Uplift of the Longmen Shan and Tibetan Plateau, and the 2008 Wenchuan (M = 7.9) earthquake. Nature 458 (7235), 194–197.

Jolivet, M., Brunel, M., Seward, D., Xu, Z., Yang, J., Malavieille, J., Roger, F., Leyreloup, A., Arnaud, N., Wu, C., 2003. Neogene extension and volcanism in the Kunlun fault zone, northern Tibet: new constraints on the age of the Kunlun fault. Tectonics 22. http://dx.doi.org/10.1029/2002TC001428.

Kidd, W.S., Molnar, P., 1988. Quaternary and active faulting observed on the 1985 Academia Sinica–Royal society geotraverse of Tibet. Philos. Trans. R. Soc. Lond. A 327, 337–363.

Kirby, E., Whipple, K.X., Burchfiel, B.C., Tang, W., Berger, G., Sun, Z., Chen, Z., 2000. Neotectonics of the Min Shan, China: implications for mechanisms driving Quaternary deformation along the eastern margin of the Tibetan Plateau. Geol. Soc. Am. Bull. 112 (3), 375–393.

Kirby, E., Harkins, N., Wang, E., Shi, X., Fan, C., Burbank, D., 2007. Slip rate gradients along the eastern Kunlun fault. Tectonics 26 (2).

Lasserre, C., et al., 1999. Postglacial left slip rate and past occurrence of M > 8 earthquakes on the western Haiyuan fault, Gansu, China. J. Geophys. Res. Solid Earth 104 (B8), 17633–17651.

Lasserre, C., Gaudemer, Y., Tapponnier, P., Mériaux, A.S., Van der Woerd, J., Daoyang, Y., Ryerson, F.J., Finkel, R.C., Caffee, M.W., 2002. Fast Late Pleistocene slip rate on the Leng Long Ling segment of the Haiyuan fault, Qinghai, China. J. Geophys. Res. Solid Earth 107 (B11).

Lease, R.O., Burbank, D.W., Zhang, H., Liu, J., Yuan, D., 2012. Cenozoic shortening budget for the northeastern edge of the Tibetan Plateau: is lower crustal flow necessary? Tectonics 31 (3).

León Soto, G., Sandvol, E., Ni, J.F., Flesch, L., Hearn, T.M., Tilmann, F., Chen, J., Brown, L.D., 2012. Significant and vertically coherent seismic anisotropy beneath eastern Tibet. J. Geophys. Res. Solid Earth 117 (B5).

Li, H., et al., 2005. Slip rate on the Kunlun fault at Hongshui Gou, and recurrence time of great events comparable to the 14/11/2001, Mw ~7.9 Kokoxili earthquake. Earth Planet. Sci. Lett. 237, 285–299.

Li, C., Zhang, P., Yin, J., Min, W., 2009. Late Quaternary left-lateral slip rate of the Haiyuan fault, northeastern margin of the Tibetan Plateau. Tectonics 28.

Luyendyk, B.P., Kamerling, M.J., Terres, R., 1980. Geometric model for Neogene crustal rotations in southern California. Geol. Soc. Am. Bull. 91 (4), 211–217.

Meade, B.J., 2007. Present-day kinematics at the India–Asia collision zone. Geology 35 (1), 81–84.

Means, W.D., 1989. Stretching faults. Geology 17 (10), 893–896.

Means, W.D., 1990. One-dimensional kinematics of stretching faults. J. Struct. Geol. 12 (2), 267–272.

Mercier, J.L., Vergely, P., Zhang, Y.Q., Hou, M.J., Bellier, O., Wang, Y.M., 2013. Structural records of the Late Cretaceous–Cenozoic extension in Eastern China and the kinematics of the southern Tan-Lu and Qinling fault zone (Anhui and Shaanxi provinces, PR China). Tectonophysics 582, 50–75.

Meyer, B., Tapponnier, P., Bourjot, L., Métivier, F., Gaudemer, Y., Peltzer, G., Shunmin, G., Zhitai, C., 1998. Crustal thickening in Gansu-Qinghai, lithospheric mantle subduction, and oblique, strike-slip controlled growth of the Tibet Plateau. Geophys. J. Int. 135 (1), 1–47. http://dx.doi.org/10.1046/j.1365-246X.1998.00567.x.

Mock, C., Arnaud, N.O., Cantagrel, J.M., 1999. An early unroofing in northeastern Tibet? Constraints from $^{40}Ar/^{39}Ar$ thermochronology on granitoids from the eastern Kunlun range (Qianghai, NW China). Earth Planet. Sci. Lett. 171 (1), 107–122.

Molnar, P., Tapponnier, P., 1981. A possible dependence of tectonic strength on the age of the crust in Asia. Earth Planet. Sci. Lett. 52, 107–114.

Onderdonk, N.W., 2005. Structures that accommodated differential vertical axis rotation of the western transverse ranges, California. Tectonics 24 (4).

Peltzer, G., Saucier, F., 1996. Present-day kinematics of Asia derived from geologic fault rates. J. Geophys. Res. Solid Earth 101 (B12), 27943–27956.

Peltzer, G., Tapponnier, P., 1988. Formation and evolution of strike-slip faults, rifts, and basins during the India-Asia collision: an experimental approach. J. Geophys. Res. Solid Earth 93 (B12), 15085–15117.

Platt, J.P., Becker, T.W., 2010. Where is the real transform boundary in California? Geochem. Geophys. Geosyst. 11 (6).

Platt, J.P., Becker, T.W., 2013. Kinematics of rotating panels of E–W faults in the San Andreas system: what can we tell from geodesy? Geophys. J. Int. 194 (3), 1295–1301.

Ramsay, J.G., Huber, M.I., 1983. The Techniques of Modem Structural Geology. Strain Analysis Vol. 1. Academic Press, London.

Ratschbacher, L., Hacker, B.R., Calvert, A., Webb, L.E., Grimmer, J.C., McWilliams, M.O., Ireland, T., Dong, S., Hu, J., 2003. Tectonics of the Qinling (Central China): tectonostratigraphy, geochronology, and deformation history. Tectonophysics 366, 1–53.

Reith, R.C., 2013. Structural geology of a central segment of the Qilian Shan-Nan Shan thrust belt. Implications for the Magnitude of Cenozoic Shortening in the Northeastern Tibetan Plateau. University of California, Los Angeles [M.S. thesis]. 73 p.

Ryan, W.B.F., Carbotte, S.M., Coplan, J.O., O'Hara, S., Melkonian, A., Arko, R., Weissel, R.A., Ferrini, V., Goodwillie, A., Nitsche, F., Bonczkowski, J., Zemsky, R., 2009. Global multi-resolution topography synthesis. Geochem. Geophys. Geosyst. 10 (8).

Sun, Z.M., Yang, Z.Y., Pei, J.L., Yang, T.S., Wang, X.S., 2006. New Early Cretaceous paleomagnetic data from volcanic and red beds of the eastern Qaidam block and its implications for tectonics of Central Asia. Earth Planet. Sci. Lett. 243, 268–281.

Tapponnier, P., Peltzer, G., Le Dain, A.Y., Armijo, R., Cobbold, P., 1982. Propagating extrusion tectonics in Asia: new insights from simple experiments with plasticine. Geology 10 (12), 611–616.

Tapponnier, P., Xu, Z., Roger, F., Meyer, B., Arnaud, N., Wittlinger, G., Yang, J., 2001. Oblique stepwise rise and growth of the Tibet Plateau. Science 294, 1671–1677.

Taylor, M., Yin, A., 2009. Active structures of the Himalayan–Tibetan orogen and their relationships to earthquake distribution, contemporary strain field, and Cenozoic volcanism. Geosphere 5, 199–214.

Thatcher, W., 2007. Microplate model for the present-day deformation of Tibet. J. Geophys. Res. Solid Earth 112 (B1).

Van Der Woerd, J., Ryerson, F.J., Tapponnier, P., Gaudemer, Y., Finkel, R., Mériaux, A.S., Caffee, M., Guoguang, Z., Qunlu, H., 1998. Holocene left-slip rate determined by cosmogenic surface dating on the Xidatan segment of the Kunlun fault (Qinghai, China). Geology 26 (8), 695–698.

Van Der Woerd, J., Ryerson, F.J., Tapponnier, P., Meriaux, A.S., Gaudemer, Y., Meyer, B., Finkel, R., Caffee, M., Guoguang, Z., Zhiqin, X., 2000. Uniform slip-rate along the Kunlun fault: implications for seismic behaviour and large-scale tectonics. Geophys. Res. Lett. 27 (16), 2353–2356.

Van Der Woerd, J., et al., 2002. Uniform postglacial slip-rate along the central 600 km of the Kunlun fault (Tibet), from ^{26}Al, ^{10}Be, and ^{14}C dating of riser offsets, and climatic origin of the regional morphology. Geophys. J. Int. 148 (3), 356–388.

Van Hinsbergen, D.J., Kapp, P., Dupont-Nivet, G., Lippert, P.C., DeCelles, P.G., Torsvik, T.H., 2011. Restoration of Cenozoic deformation in Asia and the size of Greater India. Tectonics 30 (5).

Wang, E., Burchfiel, B.C., 2004. Late Cenozoic right-lateral movement along the Wenquan fault and associated deformation: implications for the kinematic history of the Qaidam Basin, northeastern Tibetan Plateau. Int. Geol. Rev. 46 (10), 861–879.

Wang, C., Gao, R., Yin, A., Wang, H., Zhang, Y., Guo, T., Li, Q., Li, Y., 2011. A mid-crustal strain-transfer model for continental deformation: a new perspective from high-resolution deep seismic-reflection profiling across NE Tibet. Earth Planet. Sci. Lett. 306 (3), 279–288.

Wang, E., et al., 2012. Two-phase growth of high topography in eastern Tibet during the Cenozoic. Nat. Geosci. 5 (9), 640–645.

Weldon, R., Humphreys, E., 1986. A kinematic model of southern California. Tectonics 5 (1), 33–48.

Wu, C., Yin, A., Zuza, A.V., Zhang, J., Liu, W., Ding, L., 2016. Pre-Cenozoic geologic history of the central and northern Tibetan Plateau and the role of Wilson cycles in constructing the Tethyan Orogenic System. Lithosphere in press.

Yin, A., 2000. Mode of Cenozoic east–west extension in Tibet suggesting a common origin of rifts in Asia during the Indo-Asian collision. J. Geophys. Res. Solid Earth 105 (B9), 21745–21759.

Yin, A., 2006. Cenozoic tectonic evolution of the Himalayan orogen as constrained by along strike variation of structural geometry, exhumation history, and foreland sedimentation. Earth Sci. Rev. 76 (1), 1–131.

Yin, A., 2010a. Cenozoic tectonic evolution of Asia: a preliminary synthesis. Tectonophysics 488 (1), 293–325.

Yin, A., 2010b. A special issue on the great 12 May 2008 Wenchuan earthquake (M_w7.9): observations and unanswered questions. Tectonophysics 491, 1–9.

Yin, A., Pappalardo, R.T., 2015. Gravitational spreading, bookshelf faulting, and tectonic evolution of the South Polar Terrain of Saturn's moon Enceladus. Icarus 260, 409–439.

Yin, A., Taylor, M.H., 2011. Mechanics of V-shaped conjugate strike-slip faults and the corresponding continuum mode of continental deformation. Geol. Soc. Am. Bull. 123 (9–10), 1798–1821.

Yin, A., Dang, Y.-Q., Zhang, M., McRivette, M.W., Burgess, W.P., Chen, X.-H., 2007. Cenozoic tectonic evolution of Qaidam Basin and its surrounding regions (part 2): wedge tectonics in southern Qaidam Basin and the Eastern Kunlun Range. In: Sears, J.W., Harms, T.A., Evenchick, C.A. (Eds.), Whence the Mountains? Inquiries Into the Evolution of Orogenic Systems: A Volume in Honor of Raymond A. Price. Geological Society of America Special Paper Vol. 433, pp. 369–390.

Yin, A., Dang, Y.-Q., Wang, L.-C., Jiang, W.-M., Zhou, S.-P., Chen, X.-H., Gehrels, G.E., McRivette, M.W., 2008a. Cenozoic tectonic evolution of Qaidam Basin and its surrounding regions (part 1): the southern Qilian Shan–Nan Shan thrust belt and northern Qaidam Basin. Geol. Soc. Am. Bull. 120 (7/8), 813–846. http://dx.doi.org/10.1130/B26180.1.

Yin, A., Dang, Y.Q., Zhang, M., Chen, X.H., McRivette, M.W., 2008b. Cenozoic tectonic evolution of the Qaidam basin and its surrounding regions (part 3): structural geology, sedimentation, and regional tectonic reconstruction. Geol. Soc. Am. Bull. 120 (7–8), 847–876.

Yin, A., Harrison, T.M., 2000. Geologic evolution of the Himalayan–Tibetan orogen. Annu. Rev. Earth Planet. Sci. 28, 211–280.

Yuan, W., Dong, J., Shicheng, W., Carter, A., 2006. Apatite fission track evidence for Neogene uplift in the eastern Kunlun Mountains, northern Qinghai–Tibet Plateau, China. J. Asia Earth Sci. 27 (6), 847–856.

Yuan, et al., 2013. The growth of northeastern Tibet and its relevance to large-scale continental geodynamics: a review of recent studies. Tectonics 32, 1358–1370.

Zhang, P., et al., 1991. Amount and style of late Cenozoic deformation in the Liupan Shan area, Ningxia Autonomous Region, China. Tectonics 10 (6), 1111–1129.

Zhang, Y.Q., Vergely, P., Mercier, J., 1995. Active faulting in and along the Qinling range (China) inferred from SPOT imagery analysis and extrusion tectonics of south China. Tectonophysics 243 (1), 69–95.

Zhang, Y.Q., Mercier, J.L., Vergély, P., 1998. Extension in the graben systems around the Ordos (China), and its contribution to the extrusion tectonics of south China with respect to Gobi-Mongolia. Tectonophysics 285 (1), 41–75.

Zhang, P.Z., et al., 2004. Continuous deformation of the Tibetan Plateau from global positioning system data. Geology 32 (9), 809–812.

Zheng, D., et al., 2006. Rapid exhumation at ~8 Ma on the Liupan Shan thrust fault from apatite fission-track thermochronology: implications for growth of the northeastern Tibetan Plateau margin. Earth Planet. Sci. Lett. 248 (1), 198–208.

Zhu, B., Kidd, W.S.F., Rowley, D.B., Currie, B.S., Shafique, N., 2005. Age of initiation of the India–Asia collision in the east-central Himalaya. J. Geol. 113, 265–285.

Zuza, A.V., Yin, A., 2013. Ductile bookshelf faulting: a new kinematic model for Cenozoic deformation in northern Tibet. AGU Fall Meet. Abstr. 1 (2).

Zuza, A.V., Yin, A., Li, J., 2014. Deciphering the coupled Paleozoic and Cenozoic tectonic history of the Qilian Shan, northeastern Tibetan Plateau. AGU Fall Meet. Abstr. 1, 4563.

Zuza, A.V., Cheng, X., Yin, A., 2016. Testing models of Tibetan Plateau formation with Cenozoic shortening estimates across the Qilian Shan-Nan Shan thrust belt. Geosphere 12 (2), 501–532.